LPT-ORSAY 10/104, UCD-HEP-TH-2010-14

Next-to-Minimal Supersymmetric Model Higgs Scenarios for Partially Universal GUT Scale Boundary Conditions

John F. Gunion[1], Daniel E. López-Fogliani[2,3], Leszek Roszkowski[3,4] Roberto Ruiz de Austri[5], and Tom A. Varley[3]
[1] *Department of Physics, University of California at Davis, Davis, CA, USA*
[2] *Laboratoire de Physique Théorique, Université Paris-Sud, F-91405 Orsay, France.*
[3] *Department of Physics and Astronomy, The University of Sheffield, Sheffield S3 7RH, England*
[4] *The Andrzej Soltan Institute for Nuclear Studies, Warsaw, Poland*
[5] *Instituto de Física Corpuscular, IFIC-UV/CSIC, Valencia, Spain*

We examine the extent to which it is possible to realize the NMSSM "ideal Higgs" models espoused in several papers by Gunion *et al.* in the context of partially universal GUT scale boundary conditions. To this end we use the powerful methodology of nested sampling. We pay particular attention to whether ideal-Higgs-like points not only pass LEP constraints but are also acceptable in terms of the numerous constraints now available, including those from the Tevatron and B-factory data, $(g-2)_\mu$ and the relic density Ωh^2. In general for this particular methodology and range of parameters chosen, very few points corresponding to said previous studies were found, and those that were found were at best 2σ away from the preferred relic density value. Instead, there exist a class of points, which combine a mostly singlet-like Higgs with a mostly singlino-like neutralino coannihilating with the lightest stau, that are able to effectively pass all implemented constraints in the region $80 < m_h < 100$. It seems that the spin-independent direct detection cross section acts as a key discriminator between ideal Higgs points and the hard to detect singlino-like points.

Keywords: Supersymmetric Effective Theories, Cosmology of Theories beyond the SM, Dark Matter

I. INTRODUCTION

As the LHC begins its first physics runs, more scrutiny can be placed on possible regions where Beyond the Standard Model (BSM) physics can exist. One intriguing possibility is the "ideal Higgs" scenario pointed out by Gunion *et al.* [1–3]. In this Next-to-Minimal Supersymmetric Model (NMSSM) scenario, the lightest Higgs, h_1, has mass $m_{h_1} \sim 100$ GeV and SM-like couplings to WW, ZZ, but decays in such a way that LEP limits are obeyed. In general, this is possible if the h_1 decays primarily to a pair of the lightest pseudoscalar Higgs bosons, $h_1 \to a_1 a_1$, (resulting in a small branching ratio for $h_1 \to b\bar{b}$). Because $m_{a_1} < 2m_B$, the a_1 then subsequently decays to 2τ, $2g$, or $2c$, the precise mixture depending on $\tan\beta$, with 2τ being dominant at high $\tan\beta$ while all states are important at low $\tan\beta$. This allows these points to sidestep the LEP results [4] on $C^{2b}_{\rm eff}$ and $C^{4b}_{\rm eff}$, defined as:

$$\begin{aligned} C^{2b}_{\rm eff} &= |C_V(1)|^2 \times BR(h_1 \to b\bar{b}), \\ C^{4b}_{\rm eff} &\equiv |C_V(1)|^2 \times BR\left(h_1 \to a_1 a_1\right) \times \left[BR\left(a_1 \to b\bar{b}\right)\right]^2, \end{aligned} \tag{1}$$

where $|C_V(1)|^2 \equiv g^2_{h_1 ZZ}/g^2_{h_{SM} ZZ}$, where h_{SM} denotes the Higgs boson of the Standard Model. Roughly speaking, LEP constraints are evaded if $BR(h_1 \to a_1 a_1) \gtrsim 0.7$.

There are three main motivations for such a scenario.

- Precision electroweak (PEW) data is most consistent with a SM-like Higgs having mass below 100 GeV.
- There is an excess in the combined LEP data for $e^+e^- \to Zb\bar{b}$ for $M_{b\bar{b}}$ in the region $80-100$ GeV that is consistent with $BR(h_1 \to b\bar{b}) \lesssim 0.3$, as obtained for $BR(h_1 \to a_1 a_1) \gtrsim 0.7$.

- A mass $m_{h_1} \lesssim 100$ GeV is consistent with a light superparticle spectrum for which GUT scale parameters need not be fine tuned in order to obtain the correct value of m_Z at low scales.

One of the primary goals of this paper is to elucidate the extent to which the emergence of ideal-Higgs-like scenarios depends on the extent to which the pattern of soft supersymmetry breaking is highly constrained/universal.

Indeed, a key uncertainty in both the MSSM and NMSSM is the pattern of soft supersymmetry breaking, as described by the scalar masses m_0, gaugino masses $m_{1/2}$ and trilinear couplings A_0. These presumably originate from physics at some high-energy scale, e.g., from some supergravity or superstring theory, and then evolve down to lower energy scale according to well-known renormalization-group equations. What is uncertain, however, is the extent to which universality applies to the scalar masses m_0 for different squark, slepton and Higgs fields, the gaugino masses $m_{1/2}$ for the $SU(3)$, $SU(2)$ and $U(1)$ gauginos, and the trilinear couplings A_0 corresponding to different Yukawa couplings. Certain types of universality are much better motivated than others.

The suppression of flavour-changing neutral interactions suggests that the m_0 may be universal for different matter fields with the same quantum numbers, e.g., the different squark and slepton generations. However, there is no very good reason to postulate universality between, say, the spartners of left- and right-handed quarks, or between squarks and sleptons. In Grand Unified Theories (GUTs), there must be universality between fields in the same GUT multiplet, e.g., u_L, d_L, u_R and e_R in a $\mathbf{10}$ of $SU(5)$, and this would extend to all matter fields in a $\mathbf{16}$ of $SO(10)$. However, there is less reason to postulate universality between these and the Higgs fields. Nevertheless, this extension of universality to the Higgs masses (UHM) is often assumed, resulting in what is commonly termed the constrained MSSM (CMSSM) or constrained NMSSM (CNMSSM). Alternatively, there may be non-universal Higgs masses (NUHM) in the more general MSSM and NMSSM. As regards the A parameters, in the MSSM or CMSSM context it is primarily the 3rd generation A_t that matters and so universality or lack thereof does not have significant phenomenological impact. However, in the NMSSM there are two new A parameters: one, A_λ, associated with the singlet-Higgs-Higgs interaction at the superfield level; and a second, A_κ, associated with the singlet-cubed superpotential terms. Currently, there is no reason for these to have the same value as A_t. Indeed, the limit in which A_κ and A_λ are zero at the GUT scale is one in which the NMSSM has an extra $U(1)_R$ symmetry, independent of the GUT-scale value of A_t [5]. Although it can certainly be the case that the universalities assumed in the NUHM relaxation of the CMSSM and the NUHM plus A_κ, A_λ relaxation of the CNMSSM are still more restrictive than suggested by many schemes of supersymmetry breaking, comparing results incorporating such relaxations to those obtained using the most restrictive CMSSM or CNMSSM universalities provides a simplified framework for understanding what new phenomena arise when poorly-motivated restrictive boundary conditions are relaxed. In particular, we will see that in the NMSSM context relaxation of the CNMSSM boundary conditions to include NUHM and non-universality for A_λ and A_κ relative to A_t already gives rise to dramatic new physics possibilities, including the possibilities of ideal-Higgs-like scenarios and singlino-singlet dark matter scenarios. If nothing else, this shows that overly restrictive universality assumptions should be avoided in order that dramatic new physics scenarios are not "needlessly" excluded.

As referred to above, previous studies in the context of the Constrained NMSSM (CNMSSM) [6, 7], in which all A parameters and all soft-SUSY-breaking masses-squared are unified, did not find ideal-Higgs-like points. In this paper, we allow the Higgs soft masses-squared to be independent of the other (unified) soft masses-squared and we allow the soft-SUSY-breaking A_κ parameter associated with the singlet field to range freely, independent of the other A parameters (which are taken to be universal). Using the advanced scanning techniques from SuperBayeS coupled to MultiNest [8] we can efficiently scan for interesting regions of parameter space and see how often points of an ideal-Higgs nature are found and look at the many phenomenological aspects that these points entail. In addition, the power of this approach to scan over *all* interesting parameters instead of fixing crucial ones to some canonical value can provide us with some insights into the full structure of the parameter space. In particular, we will not be using fine-tuning as the defining criteria when searching for ideal-Higgs-like points. This said, our choices of parameters are influenced by [1–3] and the findings therein.

II. THE IMPLEMENTATION OF NMSSM MODEL.

The NMSSM superpotential contains a new superfield S which is a singlet under the SM gauge group $SU(3)_c \times SU(2)_L \times U(1)_Y$. (For simplicity, we use the same notation for superfields and their respective spin-0 component fields.)

$$W = \epsilon_{ij} \left(Y_u \, H_u^j \, Q^i \, u + Y_d \, H_d^i \, Q^j \, d + Y_e \, H_d^i \, L^j \, e \right) - \epsilon_{ij} \lambda \, S \, H_d^i H_u^j + \frac{1}{3} \kappa S^3 \,, \tag{2}$$

where $H_d^T = (H_d^0, H_d^-)$, $H_u^T = (H_u^+, H_u^0)$, i, j are $SU(2)$ indices with $\epsilon_{12} = 1$, while λ and κ are dimensionless couplings. With the addition of a scalar singlet superfield field, there will be five neutralinos and the Higgs content of the NMSSM is extended to include three scalar Higgses, h_1, h_2 and h_3, and two pseudoscalars, a_1 and a_2. The lightest Higgs h_1 plays an important role in the scenarios we consider here, and in particular the composition will be commented on. The state composition can be written as,

$$h_1 = S_u H_u + S_d H_d + S_s S. \tag{3}$$

The superpotential in Eq. (2) is scale invariant, and the EW scale will only appear through the soft-SUSY-breaking terms in $\mathcal{L}_{\rm soft}$, which in our conventions is given by

$$\begin{aligned} -\mathcal{L}_{\rm soft} = & \, m_{\tilde{Q}}^2 \, \tilde{Q}^* \, \tilde{Q} + m_{\tilde{U}}^2 \, \tilde{u}^* \, \tilde{u} + m_{\tilde{D}}^2 \, \tilde{d}^* \, \tilde{d} + m_{\tilde{L}}^2 \, \tilde{L}^* \, \tilde{L} + m_{\tilde{E}}^2 \, \tilde{e}^* \, \tilde{e} \\ & + m_{H_d}^2 \, H_d^* \, H_d + m_{H_u}^2 \, H_u^* H_u + m_S^2 \, S^* S \\ & + \epsilon_{ij} \, \left(A_u \, Y_u \, H_u^j \, \tilde{Q}^i \, \tilde{u} + A_d \, Y_d \, H_d^i \, \tilde{Q}^j \, \tilde{d} + A_e \, Y_e \, H_d^i \, \tilde{L}^j \, \tilde{e} + \text{H.c.} \right) \\ & + \left(-\epsilon_{ij} \lambda \, A_\lambda S H_d^i H_u^j + \frac{1}{3} \kappa \, A_\kappa \, S^3 + \text{H.c.} \right) \\ & - \frac{1}{2} \, \left(M_3 \, \lambda_3 \, \lambda_3 + M_2 \, \lambda_2 \, \lambda_2 + M_1 \, \lambda_1 \, \lambda_1 + \text{H.c.} \right) . \end{aligned} \tag{4}$$

When the scalar component of S acquires a VEV, $s = \langle S \rangle$, an effective interaction $-\varepsilon_{ij} \mu H_d^i H_u^j$ is generated, with $\mu \equiv \lambda s$.

In addition to terms from $\mathcal{L}_{\rm soft}$, the tree-level scalar Higgs potential receives the usual D and F term contributions:

$$\begin{aligned} V_D = & \, \frac{g_1^2 + g_2^2}{8} \left(|H_d|^2 - |H_u|^2 \right)^2 + \frac{g_2^2}{2} |H_d^\dagger H_u|^2 \,, \\ V_F = & \, |\lambda|^2 \left(|H_d|^2 |S|^2 + |H_u|^2 |S|^2 + |\epsilon_{ij} H_d^i H_u^j|^2 \right) + |\kappa|^2 |S|^4 \\ & - \left(\epsilon_{ij} \lambda \kappa^* H_d^i H_u^j S^{*2} + \text{H.c.} \right) . \end{aligned} \tag{5}$$

Using the minimization equations we can re-express the soft breaking Higgs masses in terms of λ, κ, A_λ, A_κ, $v_d = \langle H_d^0 \rangle$, $v_u = \langle H_u^0 \rangle$ (with $\tan\beta = v_u/v_d$), and s:

$$m_{H_d}^2 = -\lambda^2 \left(s^2 + v^2 \sin^2 \beta \right) - \frac{1}{2} M_Z^2 \cos 2\beta + \lambda s \tan\beta \left(\kappa s + A_\lambda \right) \,, \tag{6}$$

$$m_{H_u}^2 = -\lambda^2 \left(s^2 + v^2 \cos^2 \beta \right) + \frac{1}{2} M_Z^2 \cos 2\beta + \lambda s \cot\beta \left(\kappa s + A_\lambda \right) \,, \tag{7}$$

$$m_S^2 = -\lambda^2 v^2 - 2\kappa^2 s^2 + \lambda \kappa v^2 \sin 2\beta + \frac{\lambda A_\lambda v^2}{2s} \sin 2\beta - \kappa A_\kappa s \,. \tag{8}$$

We are now looking at a Lagrangian that is identical in structure to our previous work [6] but with a few important differences in terms of unification. In contrast to [6], where we took CMSSM-like boundary conditions, in the present paper, we allow the Higgs mass parameters m_{H_u} and m_{H_d} to freely vary, in a similar manner to [9]. In addition A_κ is no longer taken equal to the universal value, A_0, of the other A parameters. This freedom, specifically allowing $|A_\kappa|$ to be small, will make it possible to obtain lighter pseudoscalar and

scalar Higgs masses than in [6] that are nonetheless still allowed by collider constraints. This additional freedom in Higgs mass can be seen by looking at the tree level pseudoscalar mass matrix in the basis (A^0, S) [10]:

$$\mathcal{M}_A^2 = \begin{pmatrix} \frac{2\lambda s}{\sin 2\beta}\left(\kappa s + A_\lambda\right) & \lambda v\left(A_\lambda - 2\kappa s\right) \\ \lambda v\left(A_\lambda - 2\kappa s\right) & \lambda\left(2\kappa + \frac{A_\lambda}{2s}\right) v^2 \sin 2\beta - 3\kappa A_\kappa s \end{pmatrix}. \tag{9}$$

After diagonalization of M_A^2, there will be two mass eigenstates. The lightest state will be a mixture of the CP-odd doublet state A_{MSSM} that is present in the Minimal Supersymmetric Model and the new CP-odd component, A_S, of the complex scalar S field. We write

$$a_1 \equiv \cos\theta_A A_{MSSM} + \sin\theta_A A_S, \tag{10}$$

where the entries in M_A^2 are such that the 11 entry is the MSSM diagonal entry. From Eqs. (9) and (10) it is clear that having the freedom to vary A_κ is crucial if we want to control the mass of the singlet component independently of other parameters. Despite these changes, just as in [6] the minimisation equations, (6)-(8) will be used to fix m_S, κ, and s giving us a model with input parameters $m_{1/2}$, m_0, m_{H_u}, m_{H_d}, A_0, A_κ, $\tan\beta$ and λ, in addition to $\mathrm{sgn}(\mu)$. In particular note that in our procedure, the value of κ is an output that depends on A_κ. It is important to emphasize that in contrast to previous studies looking at the ideal-Higgs region, where scanning was done at the EW scale and run up, here all of our parameters (excluding λ) are searched over at the GUT scale and then run down. One implication is that in the studies we present here it is impossible to obtain the values of the gaugino masses in [1] for a given parameter point as we are constrained by unification considerations. That said, our choice of parameters, although constrained, leads to a scan that is practicable and is a useful starting point to perturb from in order to better satisfy, for example, fine-tuning or phenomenology.

We also present the neutralino sector since the lightest neutralino will, by assumption, play the rôle of dark matter. The mass term in the Lagrangian is given by

$$\mathcal{L}^{\chi^0}_{\text{mass}} = -\frac{1}{2}(\Psi^0)^T \mathcal{M}_{\chi^0} \Psi^0 + \text{H.c.}\,, \tag{11}$$

with $\mathcal{M}_{\chi^0}$ given by a 5×5 matrix in the basis $(\widetilde{B}, \widetilde{W}, \widetilde{H}_u, \widetilde{H}_d, \widetilde{S})$,

$$\mathcal{M}_{\chi^0} = \begin{pmatrix} M_1 & 0 & -M_Z\sin\theta_W\cos\beta & M_Z\sin\theta_W\sin\beta & 0 \\ 0 & M_2 & M_Z\cos\theta_W\cos\beta & -M_Z\cos\theta_W\sin\beta & 0 \\ -M_Z\sin\theta_W\cos\beta & M_Z\cos\theta_W\cos\beta & 0 & -\lambda s & -\lambda v_u \\ M_Z\sin\theta_W\sin\beta & -M_Z\cos\theta_W\sin\beta & -\lambda s & 0 & -\lambda v_d \\ 0 & 0 & -\lambda v_u & -\lambda v_d & 2\kappa s \end{pmatrix}, \tag{12}$$

where M_1 (M_2) denotes the soft mass of the bino (wino) and θ_W denotes the weak mixing angle. After diagonalization the lightest neutralino χ_1 (which we will denote as χ from now on) can be written as:

$$\chi = N_B\widetilde{B} + N_W\widetilde{W} + N_u\widetilde{H}_u + N_d\widetilde{H}_d + N_s\widetilde{S}. \tag{13}$$

Finally, we note that couplings of the Higgs bosons and χ to SM particle states depend upon the compositions of the former. In particular, the coupling of h_1 to WW, ZZ is given by $C_V(1) \equiv g_{h_1WW}/g_{h_{SM}WW} = S_u\sin\beta + S_d\cos\beta$ (with analogous results for h_2 and h_3) and the coupling of a_1 to $b\bar{b}$ is given by $C_{a_1b\bar{b}} \equiv g_{a_1b\bar{b}}/g_{h_{SM}b\bar{b}} = \cos\theta_A\tan\beta$.

III. OUTLINE OF THE METHOD

Following the discussion of section II, in this constrained version of the NMSSM the free parameters are given by

$$\theta = (m_{1/2}, m_0, m_{H_u}, m_{H_d}, A_0, A_\kappa, \tan\beta, \lambda)\,. \tag{14}$$

CNMSSM parameters θ	SM (nuisance) parameters ψ
$10^{-2} < m_{1/2} < 4000$ GeV	$160 < M_t < 190$ GeV
$10^{-2} < m_0 < 4000$ GeV	$4 < m_b(m_b)^{\overline{MS}} < 5$ GeV
$10^{-2} < m_{H_u} < 4000$ GeV	$0.10 < \alpha_s(M_Z)^{\overline{MS}} < 0.13$
$10^{-2} < m_{H_d} < 4000$ GeV	
$\lvert A_0 \rvert < 100$ GeV	
$\lvert A_\kappa \rvert < 10$ GeV	
$2 < \tan\beta < 20$	
$10^{-3} < \lambda < 0.7$	

TABLE I: Initial ranges for our basis parameters $m = (\theta, \psi)$.

Without loss of generality, one can choose $\lambda > 0$ [10]. However, we will also (as in our previous work) fix $\mathrm{sgn}(\mu) = +1$ and then $\mu = \lambda s$ implies $s > 0$. The "nuisance" parameters are treated in the same manner as in our previous work [6], and are shown in Eq. (15):

$$\psi = (M_t, m_b(m_b)^{\overline{MS}}, \alpha_s(m_Z)^{\overline{MS}}). \tag{15}$$

Using notation consistent with previous analyses we define our eleven dimensional *basis parameter* set as

$$m = (\theta, \psi)\,, \tag{16}$$

all of which will be simultaneously scanned over. For each choice of m a number of collider and cosmological observables are calculated. These derived variables are denoted by $\xi = (\xi_1, \xi_2, \ldots)$, which are then compared with the relevant measured data, d.

In this study we will be using the "nested sampling" method [11] as implemented in the MultiNest [12] algorithm to efficiently explore the likelihood space. Generally speaking, for this study we will be looking at points of interest irrespective of statistical considerations. MultiNest provides an extremely efficient sampler even for likelihood functions defined over a parameter space of large dimensionality with a very complex structure. (See, *e.g.*, Refs. [9, 13].)

It should be emphasised here that although nested sampling was used to obtain the points, we will be drawing no statistical inferences from the results. What in effect we are doing here is using the useful properties of the technique (especially fast scans of high dimensionality parameter spaces and the ability to simultaneously scan in *all* parameters) to get a sample of representative points for the part of the parameter space we are investigating. What is presented below then, must be viewed with some observations in mind. Firstly, although data is implemented in the scans, the trading off of poor fits in one variable for good fits in another can lead to some outlandish values for key phenomenological values. In addition as the chain has to start somewhere, an unweighted scatter plot such as we will be showing below will also show these initial, poorly fitting points. To address this, for the key points we will state more precisely what the key phenomenological values are, and in general they correspond closely to experimental values. Also, regions that have clearly unacceptable experimental values will be identified where possible.

The specific region we are investigating is defined by our range of priors which are specified in table I. The above choice of priors was influenced by previous work and the preference to focus on lower values of the soft masses in order to explore ideal-Higgs-like scenarios. This also leads us to choose a log prior, defined here as being flat in $\log m_{1/2}$, $\log m_0$, $\log m_{H_u}$ and $\log m_{H_d}$ and flat in A_0, A_κ, λ and $\tan\beta$. For the nuisance parameters we use flat priors (although this is not important as they are directly constrained by measurements) and apply Gaussian likelihoods representing the experimental observations (see table II), as before [9, 14–16].

The region specified by this set of priors is by no means a fair and even-handed exploration of the parameter space, but the aim here is to try and find points in a particular regime. In particular, allowing A_κ to be independent of A_0 (unlike in our previous paper) was very important, in addition to having non-universal soft Higgs masses ($m_{H_u} \neq m_{H_d} \neq m_0$). With this additional flexibility compared to the CNMSSM type

SM (nuisance) parameter	Mean value	Uncertainty	Ref.
	μ	σ (exper.)	
M_t	172.6 GeV	1.4 GeV	[21]
$m_b(m_b)^{\overline{MS}}$	4.20 GeV	0.07 GeV	[22]
$\alpha_s(M_Z)^{\overline{MS}}$	0.1176	0.002	[22]

TABLE II: Experimental mean μ and standard deviation σ adopted for the likelihood function for SM (nuisance) parameters, assumed to be described by a Gaussian distribution.

scan we were able to find points with the desired characteristics, although as displayed below these points are still in the minority.

Two alternate exploratory scans were implemented to better understand this region, the first being to allow a much more generous range in the parameters, and the second was to do a scan with similar constrained priors but with the unification conditions $m_{H_u} = m_{H_d} = m_0$ and $A_\kappa = A_0$ enforced, as in the so-called CNMSSM studied in [6]. The objective was to see if it was the focusing into a small region or the extra freedoms in the Higgs sector that lead to us finding points of interest. What we found is that both the freedom and the focus (especially in A_κ) seem to be important.

We compute our mass spectra and observable quantities using the publicly available NMSSMTools (version 2.1.1) that includes NMSPEC with a link to Micromegas [17]; for details see Ref. [18]. We list the observables that the current version of NMSPEC is applying to points found in the scan in Table III. The relic density Ωh^2 of the lightest neutralino is computed with the help of Micromegas, which is also linked to NMSPEC. We further use the same code to compute the cross section for direct detection of dark matter via its elastic scattering with targets in underground detectors but do not include it in the likelihood due to large astrophysical uncertainties. The likelihoods for the measured observables are taken as Gaussian about their mean values, μ as tabulated in Table III, the Gaussian widths being determined by the experimental and theoretical errors, σ and τ, respectively (see the detailed explanation in Refs. [14, 15]). In the case where only an experimental limit is available, this is given, along with the theoretical error. The smearing out of bounds and combination of experimental and theoretical errors is handled in an identical manner to Refs. [14, 15], with the notable exception of the Higgs mass and LEP limits on sparticle masses, which are calculated as a step function with values of the cross section times branching ratio (in the case of the Higgs) or mass that are within two standard deviations of the experimental limit being accepted. Finally, any points that fail to provide radiative EWSB, give us tachyons or the LSP other than the neutralino are rejected.

The above discussion does not yet include the constraints from the recent analysis by ALEPH for the $e^+e^- \to Zh$, $h \to aa \to 4\tau$ channel [19] nor the constraints from BaBar data on $\Upsilon(3S) \to \gamma a$ with $a \to \tau^+\tau^-$ [20]. These will be considered ex-post-facto. In this way, we can see what the impact of these latter constraints is upon a less biased sample of otherwise acceptable points in parameter space.

IV. RESULTS

In this section we present our numerical results from global scans, mostly in the form of scatter plots for some of the most interesting combinations of observables. Most of the figures displayed are scatter plots with three distinct populations visible on them. There are a large number of grey points in the figures that follow; these so-termed *full scan* points come from all the points obtained in the scan and are thinned by a factor of one hundred for clarity. This will also eliminate many of the outlying initial points talked about earlier. This population of points can be thought of as a representation of the general structure of the parameter space, the backdrop against which we specify points of interest.

To better display the points with $BR\left(a_1 \to b\bar{b}\right) = 0$ and $BR\left(h_1 \to a_1 a_1\right) > 0.5$ we have marked them as triangles in the relevant figures. Such points will be termed Type I points. In addition, there are points with $BR(h_1 \to b\bar{b}) < 0.5$ by virtue of substantial $BR\left(h_1 \to a_1 a_1\right)$ but for which $m_{a_1} > 2m_B$ and $BR\left(a_1 \to b\bar{b}\right) \neq 0$. These are shown by squares in the figures. We call these points Type II points. In fact, there are two subclasses of Type II points. Type IIA points are such that the light Higgs is mainly

Observable	Mean value	Uncertainties		Ref.
	μ	σ (exper.)	τ (theor.)	
$\delta(g-2)_\mu \times 10^{10}$	29.5	8.8	1	[23]
$BR(\overline{B} \to X_s\gamma) \times 10^4$	3.55	0.26	0.21	[23]
$BR(\overline{B}_u \to \tau\nu) \times 10^4$	1.32	0.49	0.38	[24]
Ωh^2	0.1099	0.0062	$0.1\,\Omega h^2$	[25]
	Limit (95% CL)		τ (theor.)	Ref.
$BR(\overline{B}_s \to \mu^+\mu^-)$	$< 5.8 \times 10^{-8}$		14%	[26]
m_h	As implemented in NMSSMTools.			[18]
sparticle masses	As implemented in NMSSMTools.			[18]
$C^{2b}_{\rm eff}$	As implemented in NMSSMTools.			[18]
$C^{4b}_{\rm eff}$	As implemented in NMSSMTools.			[18]

TABLE III: Summary of the observables used in the analysis. For more details on how these are implemented, see [14].

doublet. Type IIA points pass constraints on $C^{2b}_{\rm eff}$ and $C^{4b}_{\rm eff}$ considered individually, but may struggle to pass the overall constraint implicit in LEP data on hZ production with $h \to b's$, where $b's$ represents any final state containing one or more b quarks. This overall constraint becomes important for m_h below about 110 GeV. Because of the need to consider this overall constraint, one cannot be certain of whether or not the Type IIA points with $m_{h_1} \lesssim 110 - 112$ GeV should be eliminated without submitting them to the LEP collaborations for full analysis. Thus, we will depict them in the figures. However, in general the Type I points where $m_{a_1} < 2m_B$ are more interesting. Type IIB points are ones with $BR(h_1 \to b\bar{b}) < 0.5$, large $BR\,(h_1 \to a_1 a_1)$ and $m_{a_1} > 2m_B$ but for which the light Higgs is mainly singlet. These easily pass the LEP constraints and have other interesting properties that we shall elucidate later.

There is a third class of points, Type III, that are worth singling out. These have $BR(h_1 \to b\bar{b}) > 0.5$ but pass our primary selection criteria. As for Type II points, there are two subclasses: Type IIIA for which the h_1 is mainly doublet and S^2_s is small; and Type IIIB for which h_1 is mainly singlet, $S^2_s \sim 1$. The latter easily pass LEP limits on $C^{2b}_{\rm eff}$ and $C^{4b}_{\rm eff}$, by virtue of h_1 being mainly singlet in composition, implying very small ZZh_1 coupling. In common with Type IIB, the Higgs with SM-like coupling to WW, ZZ is instead the h_2 which must have mass and/or decays that allow it to obey all of the bounds imposed by LEP. Type IIIA points pass LEP limits by virtue of $m_{h_1} \gtrsim 114$ GeV, and are therefore not "special" in any way. Type IIIB points have $m_{h_1} \in [80 - 100]$ GeV and are particularly interesting in that they have a high probability of providing the correct value of Ωh^2. In fact, in what follows *we will include in the definition of Type III points the requirement that they yield the correct value of* Ωh^2 *within* 2σ. This will mean that Type III points will have the lowest overall χ^2 of all the points in our scans. However, they cannot explain the LEP excess in this range since, as stated before, the h_1 is for the most part decoupled and it is the h_2 which plays the role of the SM-like Higgs, and it has mass above 110 GeV. Finally, we also include in our final definition of Type III points the requirement that they satisfy the "ex-post-facto" constraints from ALEPH (on the $h_1 \to a_1 a_1 \to 4\tau$ channel) and from BaBar (from $\Upsilon(3S) \to \gamma a_1$ decays) mentioned earlier. In short, our final definition of Type III points is such that they are very consistent with *all* available experimental constraints. We explicitly state our selection criteria for the various points in Table IV.

A later table will provide a fuller list of the properties of the different classes of points.

Given the motivation for searching in those regions of parameter space that might yield ideal-Higgs scenarios, we first look at the h_1 branching ratios and $C^{2b}_{\rm eff}$. The first result is shown in Fig. 1, where we plot $C^{2b}_{\rm eff}$ as a function of m_{h_1} for our study, points from previous work by Gunion *et al.* and the experimental limits from LEP. This plot already shows that the *only* points in our scans that reproduce exactly the desired qualities ($BR\left(h_1 \to b\bar{b}\right) \to 0$ with $BR\left(a_1 \to b\bar{b}\right) = 0$) while passing all LEP constraints are precisely those with a Higgs mass in the range 80 GeV $\lesssim m_{h_1} \lesssim 100$ GeV.

In Fig. 1, one also clearly sees the Type IIA points with $m_{h_1} \gtrsim 108$ GeV and the Type IIB points with $m_{h_1} \lesssim 90$ GeV. As stated above, those of the Type IIA points that have $m_{h_1} \lesssim 114$ GeV, especially those

Point Type	$BR\left(h_1 \to b\bar{b}\right)$	$BR\left(a_1 \to b\bar{b}\right)$	S_s^2
Type I	< 0.5	$= 0$	~ 0
Type IIA	< 0.5	$\neq 0$	~ 0
Type IIB	< 0.5	$\neq 0$	~ 1
Type IIIA	> 0.5	$\neq 0$	~ 0
Type IIIB	> 0.5	$\neq 0$	~ 1

TABLE IV: Definition of various points shown in figures. In the case of Type III points, we have also required that Ωh^2 be within $\pm 2\sigma$ of the observed value and that they obey the ALEPH constraints on $h_1 \to a_1 a_1 \to 4\tau$ and the BaBar constraints on $\Upsilon(3S) \to \gamma a_1$.

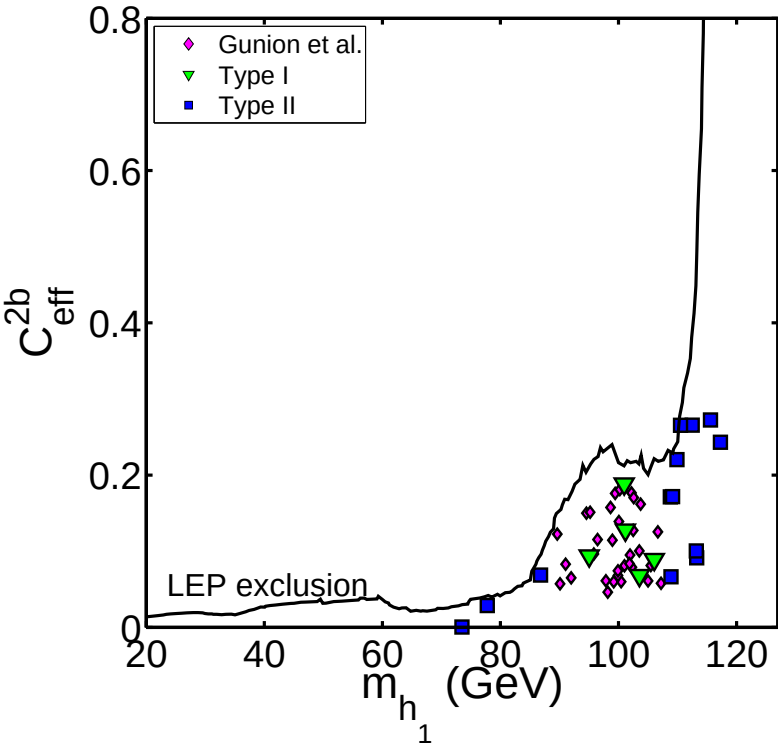

FIG. 1: A plot of the LEP limit from [4] in the $C^{2b}_{\rm eff}$ vs m_{h_1} plane, superimposed on points obtained by Gunion *et al.*in [1] and so called "Type I" points ($m_{a_1} < 2m_B$) and"Type II" points ($m_{a_1} > 2m_B$) from this study.

with $m_{h_1} \lesssim 110$ GeV, might be ruled out by a combined $Z + b's$ LEP analysis, even if not ruled out by the $C^{2b}_{\rm eff}$ and $C^{4b}_{\rm eff}$ separate limits.

We display in Fig. 2 an expanded look at this region. In the top left plot we put into context the correlation between m_{h_1} and $C^{2b}_{\rm eff}$ for Type I and Type II points by showing "background" points from the full scan. There, we see that there are many background points with $C^{2b}_{\rm eff}$ of order 0.7 to 0.8 but with large enough m_{h_1} to escape LEP limits, as characteristic of Type IIIA points, as well as background points with very low m_{h_1} and $C^{2b}_{\rm eff}$, which include Type IIIB points. Other plots in this figure show that we obtain the points with small $C^{2b}_{\rm eff}$ in two different ways. The first means is to suppress the branching ratio, $BR\left(h_1 \to b\bar{b}\right)$, as is the case with most Type I and Type IIA points. The second is to suppress the squared-coupling $|C_V(1)|^2$, as happens if the h_1 is sufficiently singlet in composition, which is the case in particular for Type IIB points. Indeed there can be a lot of points in a similar m_{h_1} region to that identified by Gunion *et al.* (*i.e.* 80 GeV $\lesssim m_{h_1} \lesssim$ 100 GeV) that escape LEP limits via suppression of $|C_V(1)|^2$ rather than via suppression

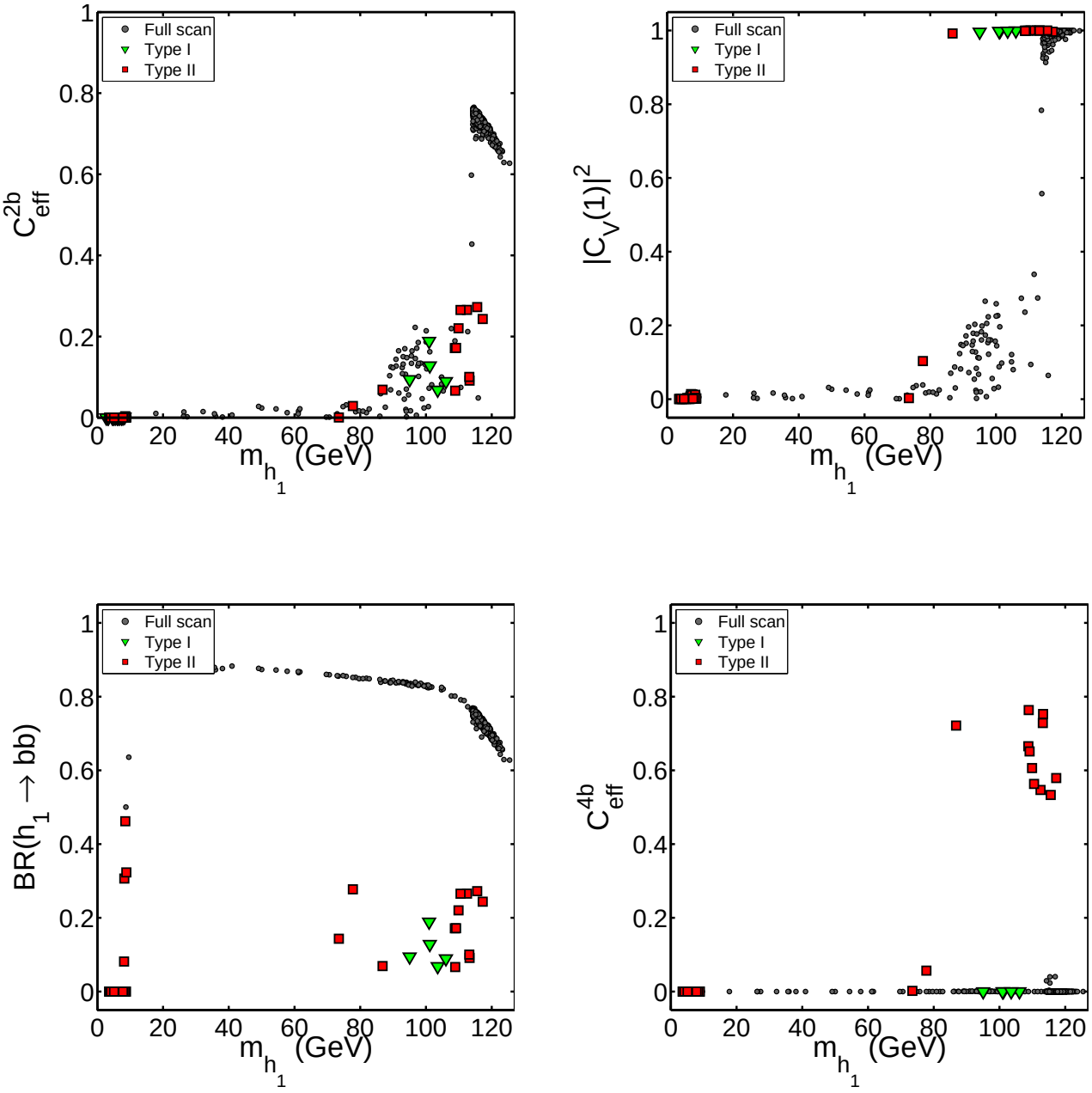

FIG. 2: Plots of various phenomenological quantities — see Eq. (1) — as a function of m_{h_1}. Note that all plots and all figures to come use the color red for the Type II points, as opposed to the coloring in Fig. 1, where the color blue was used for Type II points.

of $BR(h_1 \to b\bar{b})$. Small $|C_V(1)|^2$ implies that the h_1 cannot act as a "ideal" Higgs defined as having SM-like WW, ZZ coupling but mass $\lesssim 105$ GeV.

The bottom right figure in Fig. 2 shows $C^{4b}_{\rm eff}$ against m_{h_1}. This can be compared with a similar figure in [1]. In general it is clear that the Type I points all have $C^{4b}_{\rm eff} = 0$ (since $m_{a_1} < 2m_B$) while for Type IIA points $C^{4b}_{\rm eff}$ is quite significant and, for those points with $m_{h_1} < 114$ GeV, is not far below the LEP limit. As

noted earlier, since the limits on $C_{\rm eff}^{2b}$ and $C_{\rm eff}^{4b}$ are being applied individually and not in combination it could well be that the Type IIA points with $m_{h_1} < 114$ GeV, especially those with $m_{h_1} \lesssim 110$ GeV, are in fact in contradiction with LEP. But, without a full LEP analysis, it can be instructive to leave them in with this caveat in mind. One thing to notice in general is that the ideal-Higgs-like Type I and the Type IIA points with $m_{h_1} \lesssim 110$ GeV and fairly large $|C_V(1)| \sim 1$ are very rare, even in the context of a scan looking for these regions; this could be an artifact of our scanning technique or it could be that these points are truly hard to find given the criteria and high-scale boundary conditions we have used.

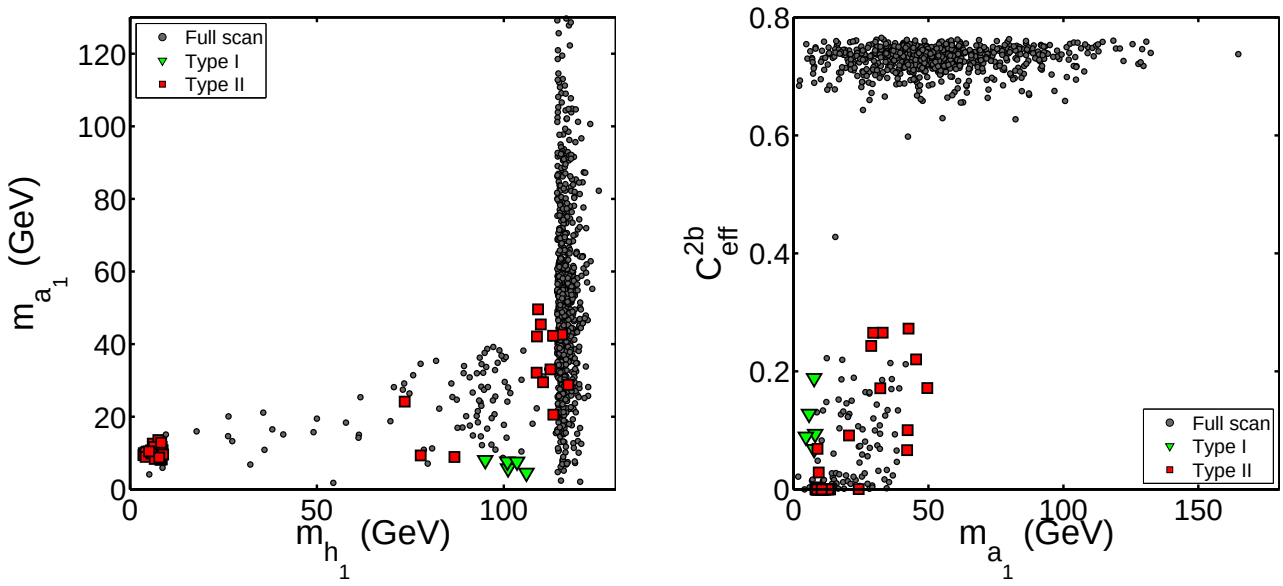

FIG. 3: Plots of m_{a_1} as a function of m_{h_1} and of $C_{\rm eff}^{2b}$ as a function of m_{a_1}.

Since m_{a_1} is so crucial to whether or not a given point is ruled out by LEP data, it is useful to understand how m_{h_1} and $C_{\rm eff}^{2b}$ correlate with m_{a_1}. In the left plot of Fig. 3 we display all the different types of points in the m_{h_1}–m_{a_1} plane. Note again the Type IIA points with $m_{a_1} > 2m_B$ and 109 GeV $\lesssim m_{h_1} < 114$ GeV that escape LEP limits on $C_{\rm eff}^{4b}$ despite having large $BR(h_1 \to a_1 a_1)$ and large $BR(a_1 \to b\bar{b})$. These also appeared in Fig. 2.

To better demonstrate the interplay between the various branching ratios needed to evade LEP constraints, some of the crucial ones are depicted in the same convention in Fig. 4. One can see that the green Type I points are clearly isolated, with the key discriminator from Type II points being $BR\left(a_1 \to b\bar{b}\right)$. In Fig. 4, some key differences between Type IIA and Type IIB points are apparent, the most notable being the very small $BR(h_1 \to a_1 a_1)$ for Type IIB (singlet h_1) points. Note also that *all* Type III points have very small $BR(h_1 \to a_1 a_1)$.

We will shortly discuss whether or not the Type I points escape the latest ALEPH limits on $h_1 \to a_1 a_1$ with $a_1 \to \tau^+\tau^-$. Such escape is possible when $\tan\beta$ is small, since at small $\tan\beta$ one predicts that $BR(a_1 \to \tau^+\tau^-)$ is significantly suppressed due to substantial branching ratios for a_1 to $c\bar{c}$, $s\bar{s}$ and gg and the resulting final states in $h_1 \to a_1 a_1$ are less strongly constrained than the $h_1 \to a_1 a_1 \to 4\tau$ final state. This was discussed in [27].

In Fig. 5 we show the square of the singlet component of the h_1, and the square of the singlino component of the lightest neutralino, the χ, as functions of m_{h_1}. These figures illustrate a number of things. First note the large number of points with $N_s^2 \sim 1$ and $S_s^2 \sim 1$, the latter implying that $|C_V(1)|^2$ is greatly suppressed. Included in this set of points are the Type IIB points with $m_{h_1} < 80$ GeV as well as the Type IIIB points with low m_{h_1}, large $BR(h_1 \to a_1 a_1)$ and non-zero $BR(a_1 \to b\bar{b})$ — all these points escape LEP limits since the h_1 is very singlet-like. Second, we observe that the S_s^2 plot is closely related to the top right panel in Fig. 2. As noted in the discussion of the latter figure, it is the Type I points and Type IIA points with

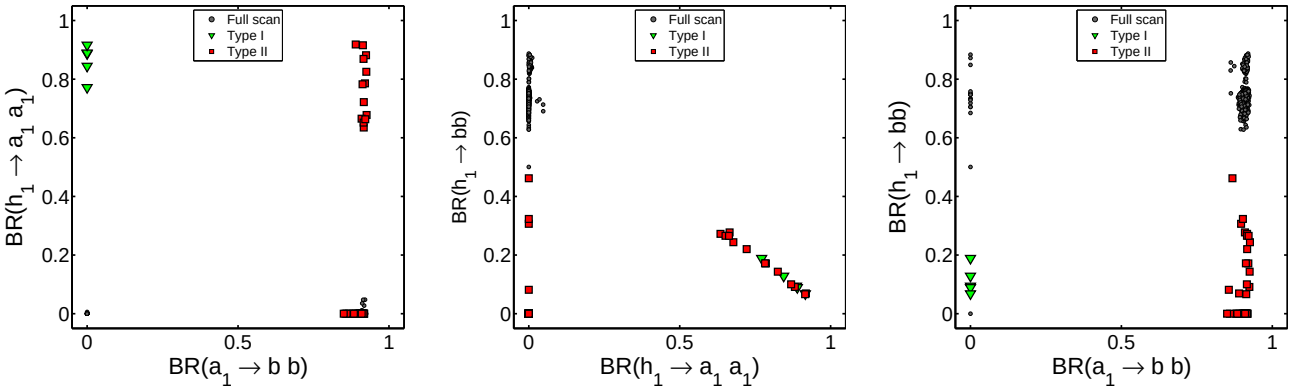

FIG. 4: Plots of: $BR(h_1 \to a_1 a_1)$ vs. $BR(a_1 \to b\bar{b})$; $BR(h_1 \to b\bar{b})$ vs. $BR(h_1 \to a_1 a_1)$; and $BR(h_1 \to b\bar{b})$ vs. $BR(a_1 \to b\bar{b})$.

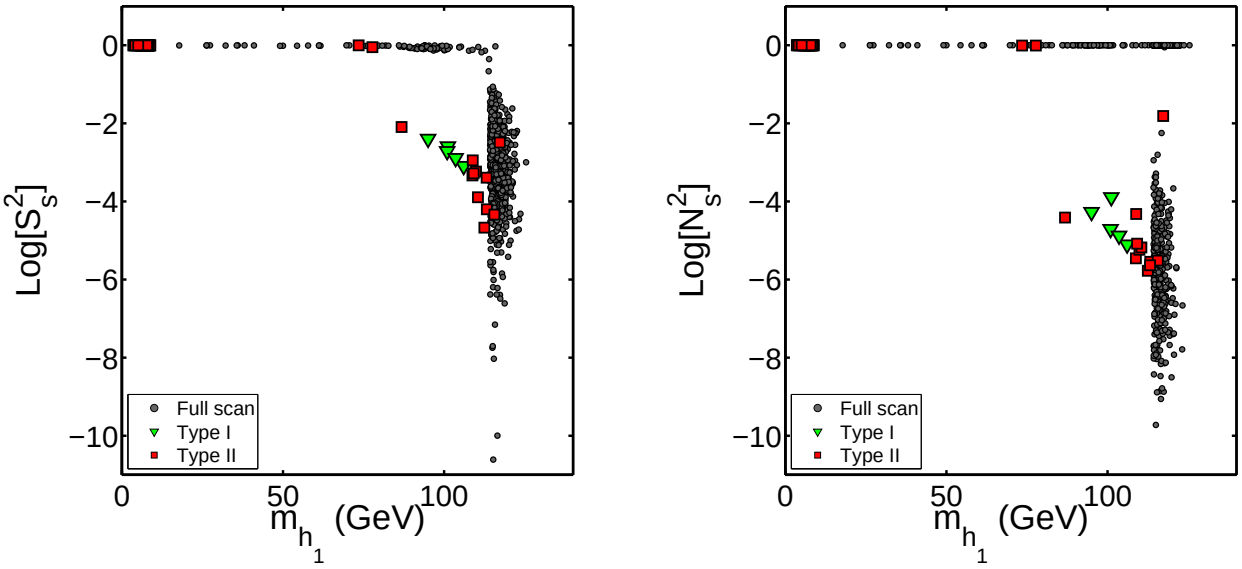

FIG. 5: We plot the square of the singlet component of the h_1 and the square of the singlino component of χ as functions of m_{h_1}.

$m_{h_1} \gtrsim 80$ GeV for which the h_1 is highly doublet-like whereas the Type IIB points with $m_{h_1} \lesssim 80$ GeV have a singlet-like h_1. And, finally, there is the large collection of points with $m_{h_1} > 114$ GeV that are unconstrained by LEP data and typically are very doublet-like.

The right hand plot of Fig. 5 will be of more use below when we consider dark matter, but it does show an interesting correlation, namely that the Type I points and the Type IIA points with $m_{h_1} \gtrsim 80$ GeV stand out by having a χ that is bino-like instead of singlino-like, the latter being more typical of the majority of points found in our scans, including Type IIB points. We further note that the Type IIIB points that have $m_{h_1} \lesssim 110$ GeV and $S_s^2 \sim 1$ also have $N_s^2 \sim 1$. In contrast, the Type IIIA points which have $m_{h_1} > 114$ GeV and small S_s^2 (with S_u^2 being large instead) can have either large N_s^2 or large N_B^2 (*i.e.* singlet-like χ or bino-like χ).

Point	m_0 (GeV)	$m_{1/2}$ (GeV)	m_{H_u} (GeV)	m_{H_d} (GeV)	A_κ (GeV)	A_0 (GeV)	λ	$\tan\beta$	G
1	452	223	3.54	543	5.69	33.7	0.481	2.54	30.4
2	10.9	287	710	180	7.89	51.7	0.436	3.61	30.9
3	7.57	467	2.23	655	-4.65	28.1	0.408	2.15	17.6
4	0.717	393	0.724	622	2.43	46.6	0.328	2.52	15.2
5	0.804	387	42.0	526	7.17	46.3	0.399	2.05	18.8

Point	$\Omega\ h^2$	$\delta(g-2)_\mu$	$BR(\overline{B}\to X_s\gamma)$	$BR(\overline{B}_s\to\mu^+\mu^-)$	m_{h_1} (GeV)	m_{a_1} (GeV)	χ^2
1	2.35	1.78×10^{-10}	3.11×10^{-4}	2.54×10^{-8}	95.0	8.04	70.3
2	0.276	10.3×10^{-10}	2.951×10^{-4}	0.127×10^{-8}	101	5.77	39.6
3	0.344	2.45×10^{-10}	3.211×10^{-4}	4.30×10^{-8}	106	4.58	30.1
4	0.341	3.90×10^{-10}	3.191×10^{-4}	3.30×10^{-8}	101	7.66	29.9
5	0.245	3.42×10^{-10}	3.391×10^{-4}	3.22×10^{-8}	104	7.63	25.7

Point	$cos\theta_A^{Max}$	$cos\theta_A$	$C^{Max}_{a_1b\bar{b}}$	$C_{a_1b\bar{b}}$	$BR\left(h_1\to a_1a_1\right)$	$BR\left(h_1\to b\bar{b}\right)$	$BR(a_1\to\tau^+\tau^-)$	$BR(a_1\to\mu^+\mu^-)$	$(\xi^2)^{Max}_{ALEPH}$	ξ^2
1	0.341	0.0186	0.867	0.0472	0.887	0.0943	0.833	0.0034	.2902	0.615 !
2	0.199	0.0197	0.719	0.0711	0.844	0.128	0.881	0.0042	.49809	0.655 !
3	0.309	0.00631	0.664	0.0136	0.890	0.0893	0.771	0.0047	.75916	0.529
4	0.336	0.00527	0.849	0.0133	0.772	0.189	0.837	0.0035	.52524	0.541 !
5	0.443	0.00716	0.906	0.0146	0.916	0.0682	0.786	0.0034	.67593	0.566

TABLE V: Displayed are some values of interest for the Type I points found in our scans. In the upper table we show the base parameters that give us our population of interesting (Type I) points. The final column, denotes G, defined in Eq. (18), a measure of the fine-tuning needed to obtain the (low) value of m_{a_1}. In the middle table are some of the phenomenological values for the points of interest. Notice the likelihood (to be precise the $-2\log(\text{likelihood}) = \chi^2$) in general is large reflecting a poor fit, and this is largely being driven by poor fits to Ωh^2 [13]. The bottom table shows some of the key branching ratios of interest for Type I points, and compares the ALEPH limits on $\xi^2 \equiv |C_V(1)|^2 \times BR\left(h_1\to a_1a_1\right)\times\left[BR(a_1\to\tau^+\tau^-\right]^2$ with the predicted values. Points appended with an exclamation mark are excluded by the ALEPH analysis. However, as discussed later, by adjusting A_κ by a very small amount they can be brought into agreement with the ALEPH limits without affecting any other phenomenology.

Full details regarding Type I points appear in Table V. The upper table shows the input parameter values for each of the Type I points. The corresponding "light-a_1" fine-tuning measure, G, defined by:

$$G \equiv Min\left\{[Max(|F_{A_\lambda}|,|F_{A_\kappa}|)],|F_{A_\lambda}+F_{A_\kappa}|\right\}, \tag{17}$$

where,

$$F_{A_\lambda} \equiv \frac{A_\lambda}{m^2_{a_1}}\frac{dm^2_{a_1}}{dA_\lambda} \qquad\qquad F_{A_\kappa} \equiv \frac{A_\kappa}{m^2_{a_1}}\frac{dm^2_{a_1}}{dA_\kappa} \tag{18}$$

is also shown. One can see some common threads for all of the Type I points. Perhaps the most intriguing is the need for λ to be quite large and away from the decoupling limit. This suggests that these points are in some sense specific to the NMSSM and are unlikely to be found in similar parametrizations of the MSSM. It is also nice to see that despite the light-a_1 fine-tuning measure G not being used in the scans, the resultant values for Type I points are not wholly unreasonable. Finally, we note that the values of $\tan\beta$ for which Type I points were found are relatively low. In the less constrained scans of parameter space performed in [1–3] Type I (ideal-Higgs) points were found at large $\tan\beta$ as well.

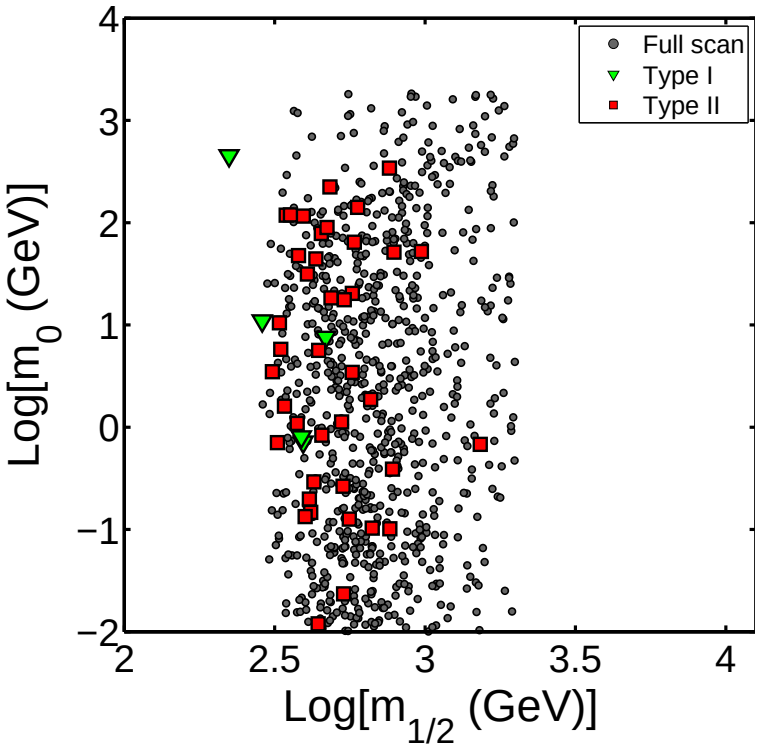

FIG. 6: A plot of our points in the m_0 — $m_{1/2}$ plane.

In Fig. 6, we show the values of m_0 and $m_{1/2}$ (at the GUT scale) for the various different types of points. We see that many of the points of Type II and Type III have quite small values of m_0 and that most Type I points have quite modest m_0. As regards $m_{1/2}$, it is typically of order $250-300$ GeV for Type I points but ranges from ~ 250 GeV up to 2 TeV for Type II and Type III points. Regardless, the resulting gluino and (non-stop) squark masses are always at least as large as 650 GeV and often significantly larger. Such values are above the limits currently being set by LHC data, which limits are typically of order $500-600$ GeV (assuming universality for the gaugino masses and for the non-Higgs scalar masses at the GUT scale). Of course, the LHC will probe gluino and squark masses of order 1 TeV after another year or two of running. In common with other models employing universality at the GUT scale, the parameter points typical of our study will then start to be ruled out.

The middle table in Table V gives some corresponding experimental values for the Type I points. It is interesting to see that the points provide phenomenologically viable results for $BR(\overline{B}\to X_s\gamma)$ and $BR(\overline{B}_s\to\mu^+\mu^-)$. However, the lower 2σ boundary for the observed $\delta(g-2)_\mu$ is $\sim 10\times 10^{-10}$ and only Type I point 2 barely predicts this high a value, the other Type I points predicting values in the range $(1.78-3.90)\times 10^{-10}$. The relic density is equally problematical, with the best value barely getting to within 2σ of the WMAP value. The likelihood is dominated by this contribution as in general the relic density is the strongest constraint on the parameter space [13]. Hence, the points with best likelihood correspond to Ωh^2 closest to its experimental value. As discussed shortly, the Type IIIB points (*i.e.* points $m_{h_1}\lesssim 104$ GeV that escape LEP limits by virtue of the h_1 being mainly singlet) quite readily achieve an Ωh^2 near the WMAP value; as a result, the χ^2 for Type IIIB points ranges from a low of ~ 1.9 to a high of ~ 6, vs. the best value of ~ 26 found for Type I points in our scans. Type IIIA points have χ^2 values only slightly larger than Type IIIB points and definitely below 26, as consistent with our requirement that Type III points be consistent with the observed Ωh^2 within $\pm 2\sigma$. Note that small χ^2 can be achieved within the other defining characteristics for Type IIIA and Type IIIB points because small Ωh^2 is possible despite the singlino or bino nature of the χ by virtue of near mass degeneracy of the χ and $\widetilde{\tau}_1$.

The bottom table of Table V gives the values of the coupling $C_{a_1 b\bar{b}} \equiv \tan\beta \cos\theta_A$ in comparison to the maximum absolute value allowed by BaBar data in the $\Upsilon_{3S} \to \gamma\tau + \tau^-$ channel. Here, $\cos\theta_A$ is the doublet component of a_1 as defined by $a_1 = \cos\theta_A a_{MSSM} + \sin\theta_A a_S$. This bottom table also gives the value of $\xi^2 \equiv |C_V(1)|^2 \times BR\,(h_1 \to a_1 a_1) \times [BR(a_1 \to \tau^+\tau^-]^2$ in comparison to the upper limit for each point from the recent ALEPH analysis. We observe that the Type I points have no problem obeying the limits from BaBar but that the ALEPH limits are very problematical for three out of five of the Type I points. However, we show below that a very small change in A_κ will bring these points into agreement with the ALEPH limits without affecting any other phenomenology. We also wish to note that the ALEPH constraints are much stronger than what was expected on the basis of Monte Carlo and so, in our opinion, some relaxation of the ALEPH bounds could be considered. If $\sim 1\sigma$ relaxation is allowed, then all our Type I points survive "as is". We also wish to note that $C^2_{a_1 b\bar{b}} \times BR(a_1 \to \mu^+\mu^-)$ roughly determines the ability to detect $gg \to a_1 \to \mu^+\mu^-$ at hadron colliders [28]. Very roughly, in the $m_{a_1} < 2m_B$ region where $BR(a_1 \to \mu^+\mu^-) \sim (0.003 - 0.005)$ detection will only be "easy" if $|C_{a_1 b\bar{b}}| \geq 1$. Unfortunately, for our Type I points, $|C_{a_1 b\bar{b}}|$ is always small, with point 2 providing the largest value of ~ 0.07.

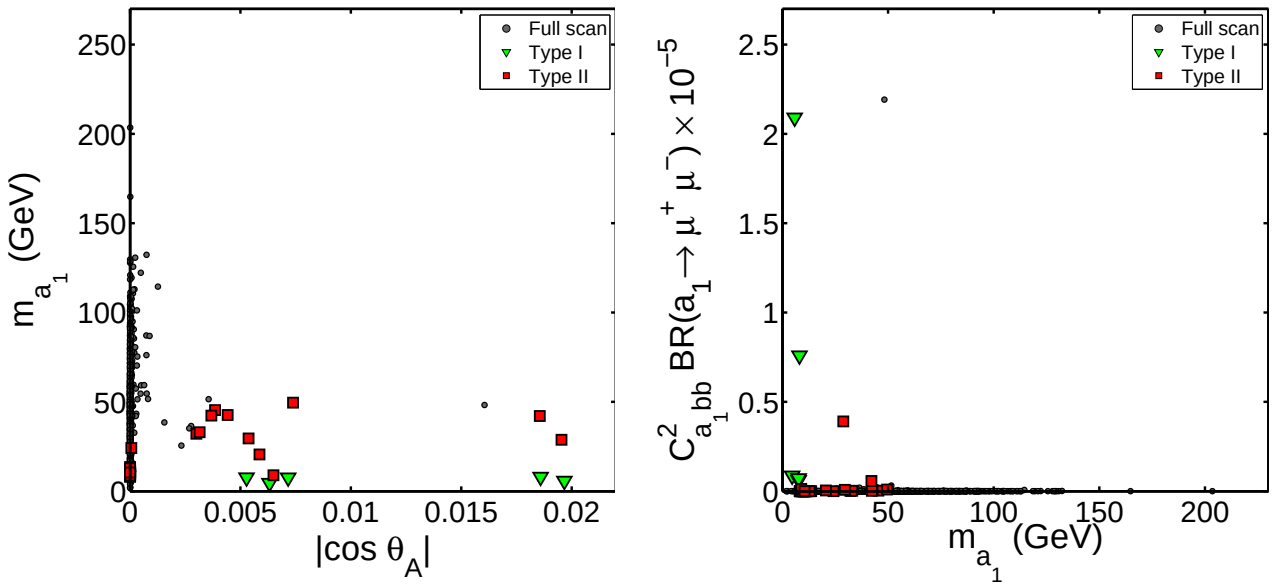

FIG. 7: We plot m_{a_1} as a function of its singlet component, $|\cos\theta_A|$ and $C^2_{a_1 b\bar{b}} BR(a_1 \to \mu^+\mu^-)$ as a function of m_{a_1}.

A more global picture of $|\cos\theta_A|$ and $C^2_{a_1 b\bar{b}} BR(a_1 \to \mu^+\mu^-)$ is provided by Fig. 7. In the left plot, we give m_{a_1} as a function of the magnitude of its singlet component, $|\cos\theta_A|$, for all points in order to show more generally how singlet the a_1 is for the different classes of points. We observe that the a_1 is extremely singlet for the vast bulk of points, including the Type IIB and Type IIIB points. This correlates with the fact that the h_1 is mainly singlet for these same two types of points.

In the right plot of Fig. 7 we show $C^2_{a_1 b\bar{b}} BR(a_1 \to \mu^+\mu^-)$ as a function of m_{a_1} to indicate which points have a reasonable probability that the production/decay channel $gg \to a_1 \to \mu^+\mu^-$ could be detected. Points for which this product is $\gtrsim 0.001$ would have a viable signal at the LHC for accumulated luminosities of order 10 fb^{-1} [28] (more being required if m_{a_1} is in the region of the Υ resonances). We see that none of our points are even close to allowing such detection.

Of course, the size of $C_{a_1 b\bar{b}}$ derives both from $\cos\theta_A$ and $\tan\beta$. Thus, it is perhaps useful to display $\tan\beta$ as a function of m_{a_1} and m_{h_1}. This is done in Fig. 8. We see that only the Type I and the Type IIA points

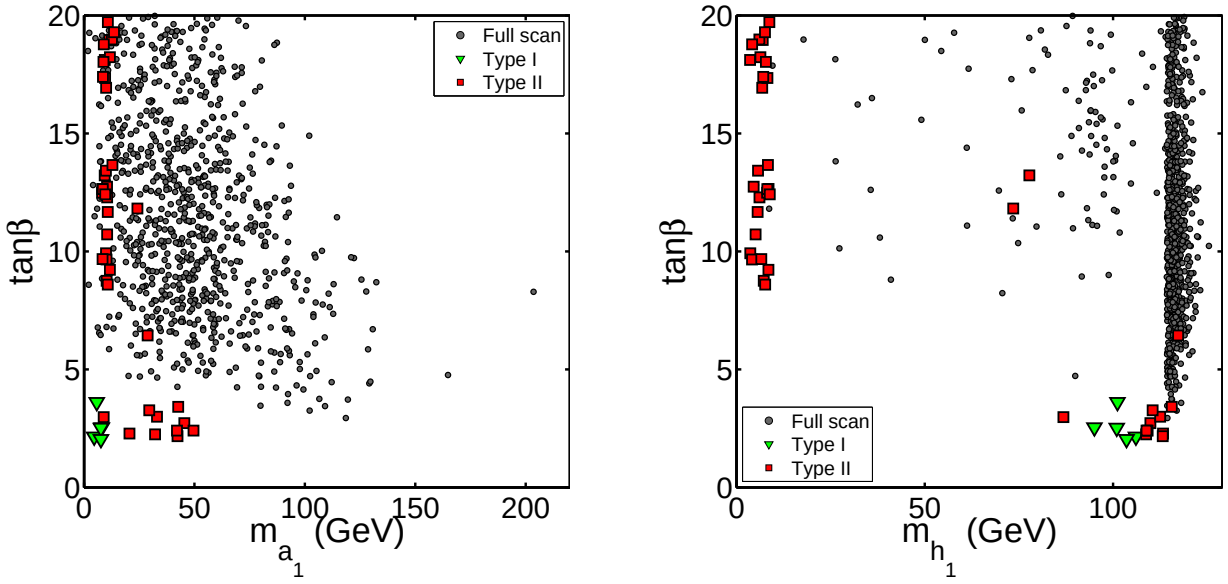

FIG. 8: We plot $\tan\beta$ vs. m_{a_1} and vs. m_{h_1}.

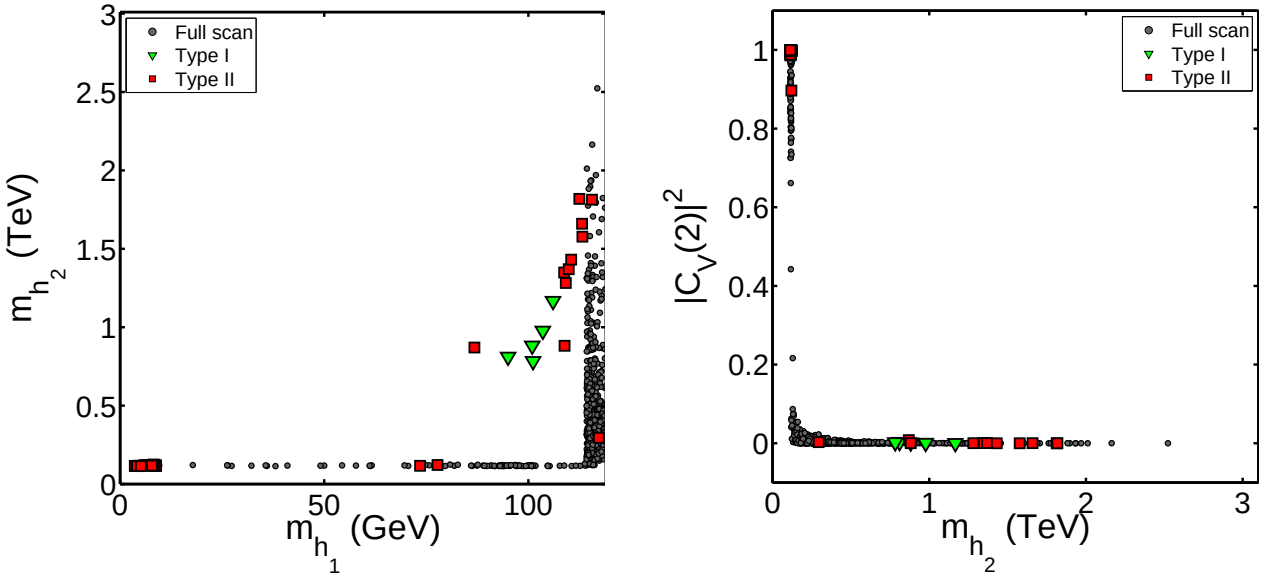

FIG. 9: We plot our points in the m_{h_2} – m_{h_1} and show $|C_V(2)|^2$ as a function of m_{h_2}.

with $m_{h_1} \gtrsim 80$ GeV (for which the a_1 and h_1 have at least a modest doublet component) are forced into the low $\tan\beta$ region. In contrast, Type IIB and Type IIIB points all have $\tan\beta > 8$. Type IIIA points can have any $\tan\beta$ above ~ 3. In the left plot of Fig. 9 we show how all the points are distributed in the m_{h_2} – m_{h_1} plane. This plot shows very clearly two branches for all the points that are neither Type I nor Type IIA points. The vertical branch corresponds to Type IIIA points where $m_{h_1} \gtrsim 114$ GeV (thereby escaping LEP limits) with $|C_V(1)|^2 \sim 1$ (see Fig. 2). The horizontal branch encompasses the Type IIB and Type IIIB points for which the h_1 is very singlet and it is instead the h_2 that is SM-like with $m_{h_2} \gtrsim 114$ GeV and $|C_V(2)|^2 \sim 1$, as displayed in the right plot of Fig. 9. Finally, we remark that $BR(h_2 \to a_1 a_1)$ is very small for all points — this is perfectly OK since LEP limits for the h_2 are evaded either because it is very singlet

or because $m_{h_2} > 114$ GeV — the extra $h_2 \to a_1 a_1$ decay channel is not needed.

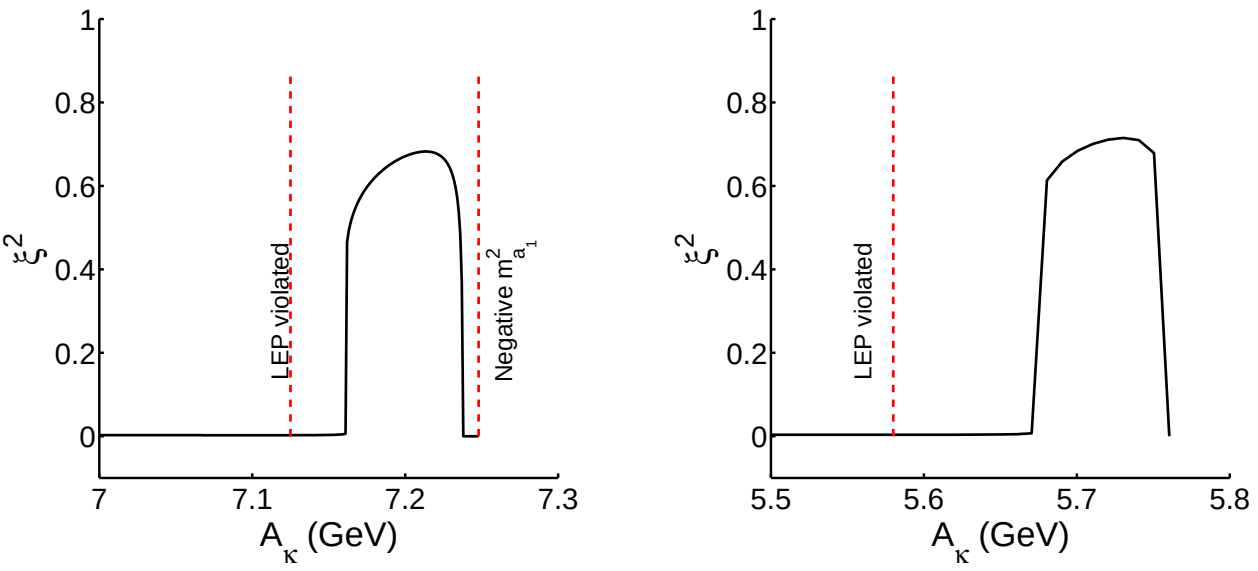

FIG. 10: The effect of varying the A_κ parameter of point 5 (left) and point 1 (right) in table V.

Let us now return to the ALEPH limits on $\xi^2 = |C_V(1)|^2 BR(h_1 \to a_1 a_1)[BR(a_1 \to \tau^+\tau^-)]^2$. In Fig. 10, we show specifically the effect of varying A_κ on ξ^2. One can see that there exist two "discontinuities" as A_κ is varied. These arise because m_{a_1} decreases with increasing A_κ . The first abrupt change occurs at the upper range of A_κ plotted when m_{a_1} passes below $2m_\tau$, and ξ^2 goes to zero because $BR(a_1 \to \tau^+\tau^-) = 0$. The 2nd abrupt change arises as A_κ is decreased and m_{a_1} becomes larger than $2m_B$. In this region, the dominant decay channel for the lightest Higgs is $h_1 \to a_1 a_1 \to 4b$ and $BR(h_1 \to a_1 a_1 \to 4\tau)$ is very small. As A_κ decreases just a little bit more, the model point in question will start to exceed LEP bounds on the $h_1 \to 4b$ final state. As seen in the left hand plot of Fig. 10, in the case of point 5 the LEP bound on C^{4b}_{eff} comes into play quite quickly as A_κ is decreased. In comparison, the right hand plot shows that in the case of point 1 there is a larger range of A_κ for which the LEP bound on C^{4b}_{eff} is satisfied *and* $\xi^2 = 0$ so that the ALEPH bound is automatically satisfied. Of course, the nominal value of A_κ from Table V for point 5 (the left-hand plot) is such that the ALEPH bound is satisfied and no adjustment of A_κ is required. We presented the plot to show how sensitive the LEP phenomenology is to A_κ. In this case, the value of A_κ can be changed somewhat from its nominal Table V value without immediately encountering a problem with either the LEP bound on the $4b$ final state or the ALEPH bound on ξ^2. In contrast, the nominal value of A_κ for point 1 in Table V gives a value for ξ^2 that is considerably too large in comparison to the $\xi^2 \leq 0.29$ ALEPH limit. In this case, we must lower A_κ in order to satisfy the ALEPH bound. Roughly, any A_κ above 5.58 GeV, the value at which the LEP $4b$ bound (dashed line) becomes relevant, but below about 5.67 GeV (vs. the nominal value of 5.69 GeV) would be allowed.

The above discussion illustrates that acceptable ξ^2 can be obtained for the type I points 1, 2 and 4 by very small shifts in A_κ that do not any way affect the remainder of the phenomenology of these points. Of course, it must be acknowledged that there is a certain level of fine-tuning of A_κ involved in getting m_{a_1} into an allowed range. This is, in fact, already reflected in the somewhat large G values of points 1 and 2 of Table V, these points being ones where the nominal ξ^2 is substantially above the ALEPH limit. Point 4 has a much more modest G value and correspondingly a broader range of A_κ would allow it to satisfy the ALEPH limit that is only slightly below the value of ξ^2 predicted by the nominal A_κ value tabulated in Table V.

As stated earlier, Ωh^2 plays a pivotal role in determining the likelihood of a given point in parameter space. Fig. 11 shows us that the range of values for Ωh^2 is huge, with many points having relic densities that are too large by orders of magnitude. In this context, the fact that Type I points tend to achieve the

right order of magnitude seems quite remarkable. That said, despite the relic density constraint pushing our scanning quite strongly towards the WMAP value, we did not find Type I points with a relic density that is less than two sigma away from the observed value. Similar remarks apply to the Type IIA points. In contrast, Type IIB points (for which the χ is very singlino-like) have much too large Ωh^2 as a result of too small an annihilation cross section.

As noted already, Type III points were defined by requiring not only $BR(h_1 \to b\bar{b}) > 0.5$ and $m_{a_1} > 2m_B$ (so that $BR(a_1 \to b\bar{b}) \neq 0$) but also by demanding that Ωh^2 is within $\pm 2\sigma$ of the observed value. Thus, it is mainly the Type III points that populate the band in the right-hand expanded plot of Fig. 11. It turns out that for all the Type III points the dominant process responsible for getting correct Ωh^2 is coannihilation of the χ with $\widetilde{\tau}_1$ — they are quite closely degenerate in mass for all the Type IIIA and Type IIIB points. In the case of points where the χ is very singlino-like, which comprises all Type IIIB points and a sizable fraction of Type IIIA points, the mass difference between χ and $\widetilde{\tau}_1$ is at most about 4 GeV and the common mass is typically of order 120 GeV. The χ has just enough gaugino and higgsino components (of order 10^{-6} at the probability level) to couple effectively and coannihilate with the $\widetilde{\tau}_1$ to get the right relic density. In the case of the Type IIIA points, for which the χ is mainly bino-like, the common mass is most often > 250 GeV (but not always) and for such points the mass difference is more typically of order 10 GeV. The very smallest χ^2 values are achieved for the Type IIIB points for which both the h_1 and the χ are mainly singlet and singlino, respectively, the "singlet-singlino" (or SS) scenario. The ease with which such low χ^2 points were found in our scans suggest that the SS scenario for dark matter should be taken quite seriously as possibly being the correct paradigm for dark matter.

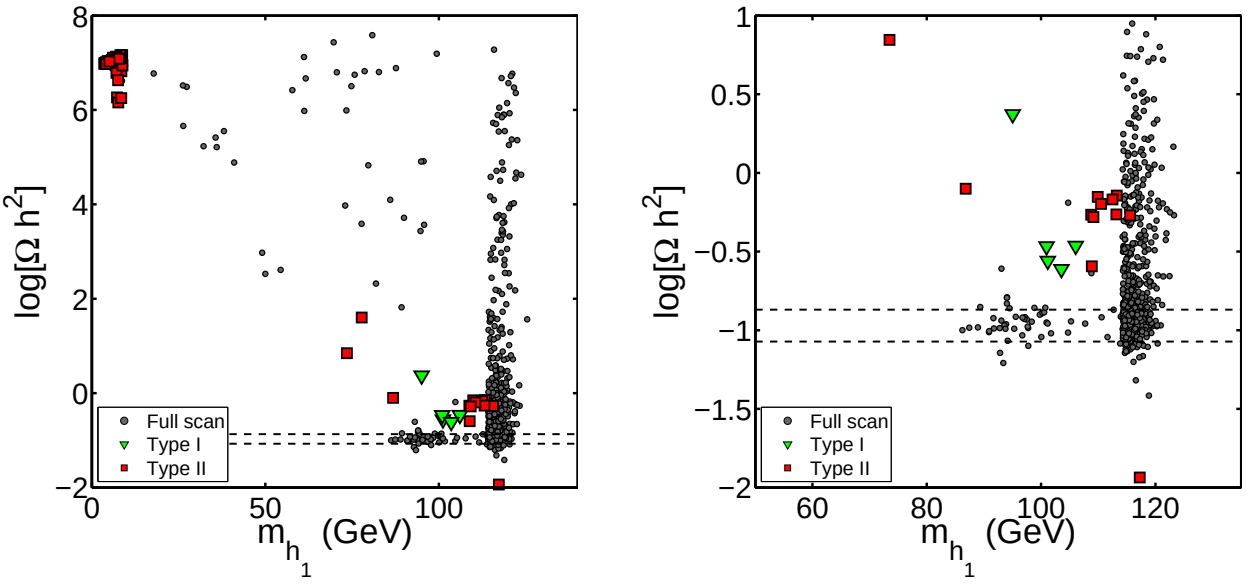

FIG. 11: The relic density, $\log(\Omega\, h^2)$, versus m_{h_1},

One question is whether small parameter changes for the Type I points could bring the predicted Ωh^2 into close agreement with observation. After all, our scans might just be slightly missing Type I points with the right relic density. To examine this, an attempt to vary the gaugino masses independently at the GUT scale was made to see if this could lead to the right amount of dark matter. In general it is not difficult to get to $\Omega h^2 \sim 0.1$, but in all the cases studied, it comes at the price of exceeding LEP limits on several channels, including Higgstrahlung processes such as Zh_1 production with $h_1 \to b\bar{b}$.

In order to do this perturbation, we took the most promising Type I point (*i.e.* the one with the best relic density value, point 5 in table V) and perturbed M_2 away from universality at the GUT scale. The results are shown in Figs. 12 and 13. What seems to be happening here is that as M_2 changes in this region, m_{a_1} also changes dramatically, so much so that perturbing M_2 by only a few GeV gives us a point that is ruled

out by the $h \to aa \to 4b's$ limit from LEP. As M_2 gets bigger, eventually we get to the crucial point where $BR\left(a_1 \to b\bar{b}\right)$ is kinematically suppressed as m_{a_1} is sufficiently light.

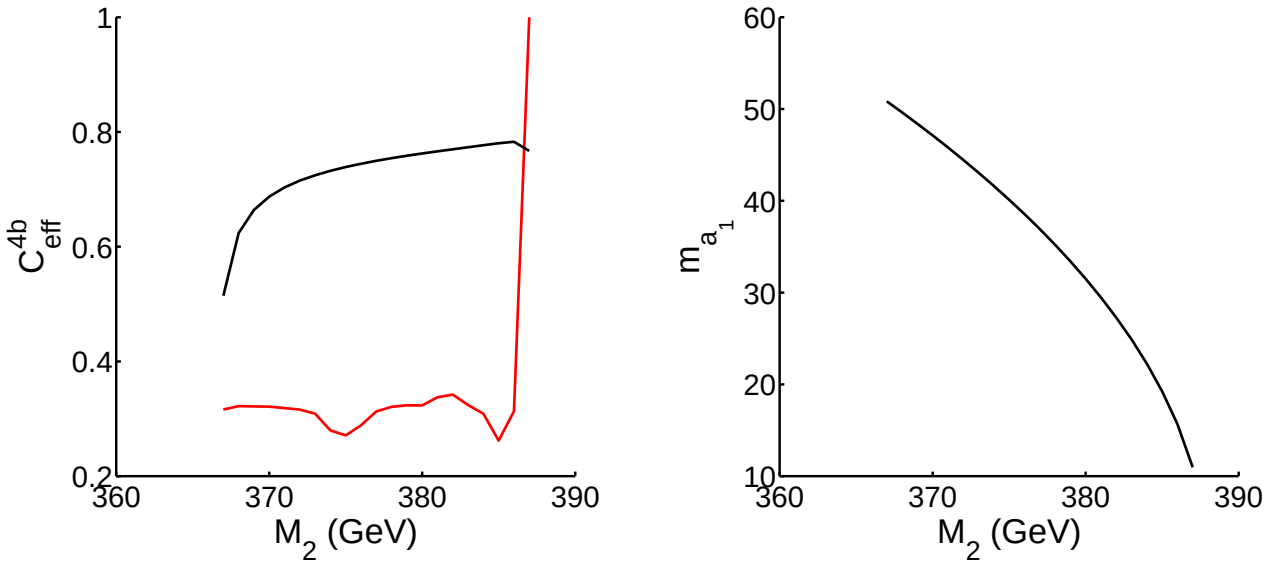

FIG. 12: The effect of varying the M_2 parameter of point 5 in table V. The left-hand plot gives the values for C^{4b}_{eff} as defined in Eq.(1) with red denoting the experimental limit and black the NMSSM predicted value as a function of M_2. The black curve terminates as M_2 increases when $m^2_{a_1}$ becomes negative. The sharp rise in the experimental limit occurs as m_{a_1} approaches and then falls below $2m_B$, the point at which the $a_1 \to 2b$ decay mode becomes kinematically forbidden. On the right, we show the rather dramatic change of m_{a_1} with M_2. In contrast, m_{h_1} remains roughly at 102 GeV over this range of M_2.

The curves in Fig. 12 do not extend below $M_2 \sim 367$ GeV or so, since, as seen in Fig. 13, in this region one exceeds the LEP limits on $C^{2b}_{\rm eff}$. In addition, the sensitivity of m_{a_1} means that soon after getting to a point where LEP limits are respected, (the exact point being unclear due to the resolution of the exploration done) m_{a_1} is driven tachyonic. Looking at this admittedly very specific case, one can perhaps begin to understand why we are obtaining so few points that are Type I and anywhere near the right relic density, given that m_{a_1} is very sensitive to changes and is the crucial element here. This is by no means a blanket statement about points being ruled out, merely an observation for this specific situation. For further study, a scan with all the gaugino masses disunified might be useful to shed light on this.

Let us now turn to predictions for direct detection of the neutralino via scattering on nucleons. In Fig. 14 we show the spin-independent cross section as a function of both m_χ and m_{h_1}, and see something not entirely unexpected: the large swathe of singlino points, which comprise Type IIB, Type IIIB and a sizable fraction of Type IIIA points, will be nearly undetectable in any upcoming direct detection experiment, having cross sections of at most 10^{-12} pb or so. On the other hand, about half the Type IIIA points have $\sigma_p^{SI} > 10^{-10}$ pb, with some having $\sigma_p^{SI} \sim 10^{-7}$ pb (and good Ωh^2). And, we should again note that all Type IIIA points have $m_{h_1} > 114$ GeV. In contrast, the Type I and Type IIA points have $m_{h_1} < 114$ GeV and often $m_{h_1} \sim 100$ GeV, *i.e.* in the m_{h_1} region of interest for explaining the LEP excess near 100 GeV. As apparent from Fig. 14 these points for which the h_1 is doublet-like seem to have a large, or at least measurable, direct detection cross section. As a result, if a largish value of σ_p^{SI} is eventually observed, the value of m_{h_1} could be used to distinguish between the Type IIIA and Type I/IIA regions of parameter space. Note that *a priori* there is no reason for Type I and Type IIA points to have a direct detection cross section that is both high enough to be tested by future experiments and low enough to avoid current constraints, and as such it is

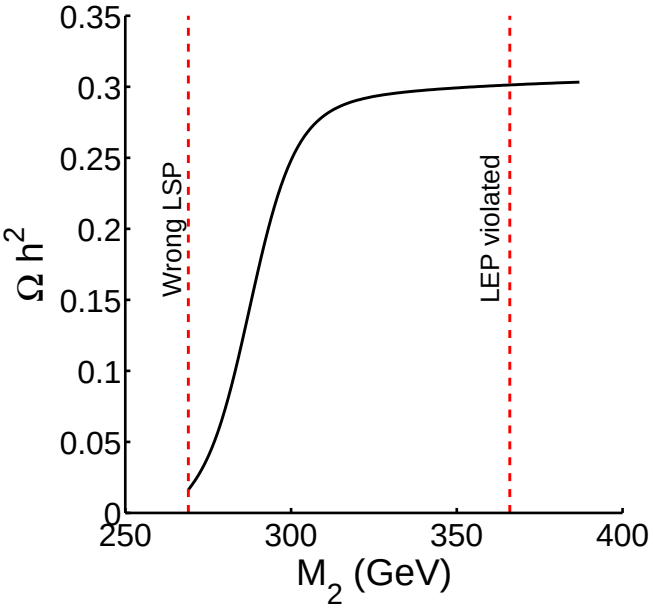

FIG. 13: The effect of varying the M_2 parameter on point 5 in table V. Here we show the change in the relic density, Ωh^2. It is possible to bring DM in line with experiment, but in doing so one violates LEP limits on several channels, below $M_2 \sim 360$ GeV in this case, which is the reason that the curves in the previous figures don't go below this value.

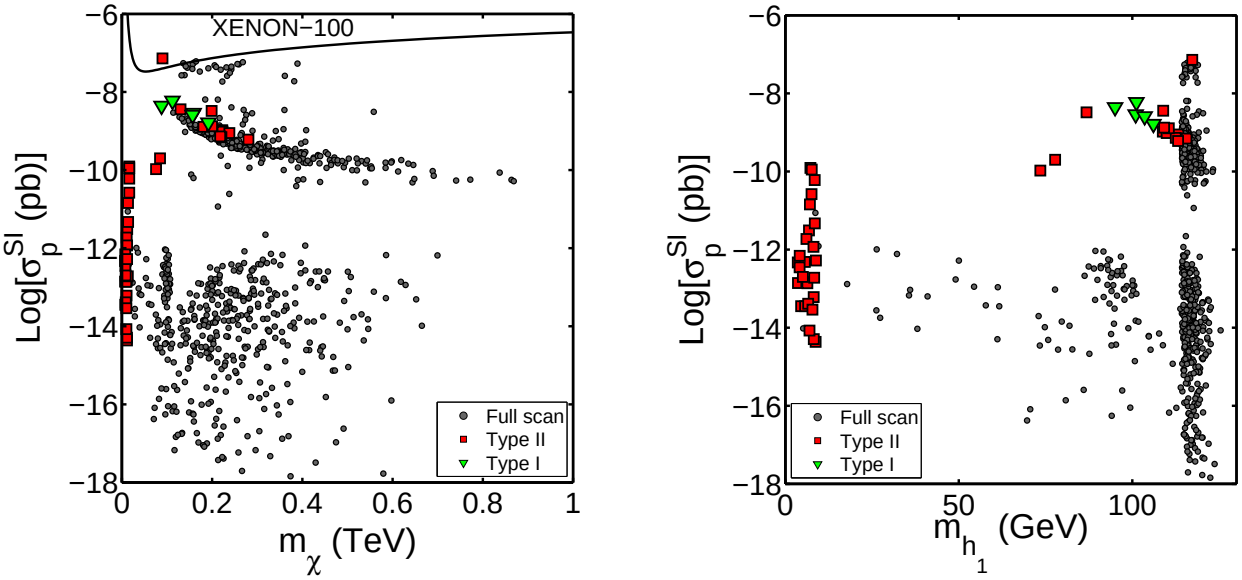

FIG. 14: The dark matter spin-independent cross section σ_P^{SI} as a function of, on the left, m_χ and, on the right, m_{h_1}. Included on the left hand side is an illustrative limit from the Xenon-100 direct detection experiment [29].

interesting to note that many such points do appear.

On another note, by comparing between the two figures in Fig. 14, we can again detect the correlation between singlet-like Higgses and singlino-like neutralinos that was apparent in Fig. 5 for values of the Higgs mass in the range $m_{h_1} < 90$ GeV. As already apparent in Fig. 5, for $114 > m_{h_1} > 90$ GeV the situation

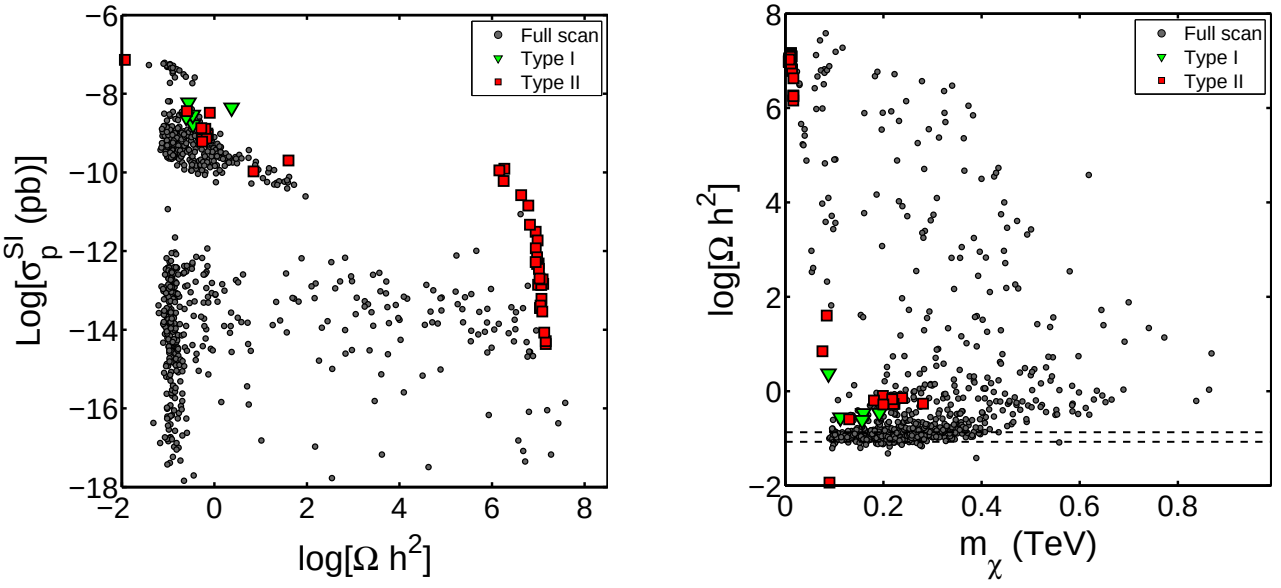

FIG. 15: Left: The spin-independent cross section, $\log(\sigma_p^{SI})$, vs. the relic density, $\log(\Omega\, h^2)$. Right: $\log(\Omega\, h^2)$ vs. m_χ.

is more complicated and there is no clear correlation between the singlet nature of the h_1 and the singlino nature of the χ.

It is interesting to comment on results for σ_p^{SI} for points with very low $m_\chi \lesssim 15$ GeV. We see in Fig. 14 that the Type IIB points are those that populate the very low m_χ region. However, these points all have a singlino-like χ and, correspondingly, the largest cross section is of order $\sigma_p^{SI} \sim 10^{-10}$ pb, *i.e.* far below the region that is needed to explain the possible CoGeNT [30] and DAMA [31] excesses in the 6 GeV $\lesssim m_\chi \lesssim$ 9 GeV region for which $\sigma_p^{SI} \gtrsim 10^{-4}$ pb is required [32]. In [33], it is shown that if one ignores GUT-scale unification then values of σ_p^{SI} within a factor of 10 of the above range are possible while still having a Higgs with SM-like WW, ZZ couplings that is sufficiently light to achieve "ideal-like" agreement with precision data. From the study presented in the present paper, it seems that such large values of σ_p^{SI} cannot be achieved in the context of the relaxed-CNMSSM boundary conditions employed here. In particular, very low m_χ values for a bino-like χ (which allowed for the largest σ_p^{SI} values in [33]) require small M_1 values, a region that is quite inaccessible in the strict CNMSSM context.

Before concluding, we provide a tabular summary of the most important characteristics of the five different classes of points that we have particularly focused on: Type I, Type IIA, Type IIB, Type IIIA and Type IIIB.

V. CONCLUSION AND SUMMARY

In the version of the NMSSM studied in this paper, we have relaxed the unification condition of A_κ and of the Higgs soft masses m_{H_u} and m_{H_d} (at the GUT scale) with respect to the CNMSSM in order to explore the extent to which the absence of the ideal-Higgs-like scenarios in the CNMSSM scans depended upon these particular (rather unmotivated) universality assumptions. Allowing for non-universal A_κ and non-universal Higgs soft masses, five parameter space points corresponding to the so called "ideal Higgs" scenario were indeed found, although these were far outnumbered by other points. The phenomenology of the ideal-Higgs points was studied, and in the context of this particular scan these points were seemingly acceptable in terms of flavour observables like $BR(\overline{B} \to X_s\gamma)$ and $BR(\overline{B}_s \to \mu^+\mu^-)$ (with $(g-2)_\mu$, in common with every other scan we have done, struggling to fit the observed 3σ difference relative to the SM). However, only two of the five ideal-Higgs-like points we found are strictly consistent with the latest ALEPH limits on the Higgs to

TABLE VI: Important characteristics of the different classes of points. The top entries in the Table list the requirements imposed in defining the classes. The bottom entries list the resulting properties of points in the different classes. Three additional requirements are imposed for Type III points (only): (i) that Ωh^2 be within 2σ of the observed value (roughly $\log[\Omega h^2] \sim -1$); (ii) ALEPH limits on $h_1 \to a_1 a_1 \to 4\tau$ are satisfied; and (iii) BaBar limits on $\Upsilon(3S) \to \gamma a_1$ are satisfied.

	Type I	Type IIA	Type IIB	Type IIIA	Type IIIB
$BR(h_1 \to b\bar{b})$	< 0.3	< 0.5	< 0.5	> 0.5	> 0.5
$BR(a_1 \to b\bar{b})$	0	$\neq 0$	$\neq 0$	$\neq 0$	$\neq 0$
S_s^2	~ 0	~ 0	~ 1	~ 0	~ 1
$\lvert C_V(1)\rvert$	~ 1	~ 1	$\ll 1$	~ 1	$\ll 1$
m_{h_1}	$\in [95, 108]$	> 75	< 90, mostly < 20	$\gtrsim 114$	< 110
m_{a_1}	$< 2m_B$	$\in [2m_B, 50]$	$\in [2m_B, 20]$	$> 2m_B$	$\in [2m_B, 40]$
$BR(h_1 \to a_1 a_1)$	> 0.7	> 0.6	~ 0	< 0.1	~ 0
N_s^2	$\ll 1$	$\ll 1$	~ 1	$\ll 1$ or ~ 1	~ 1
N_B^2	~ 1	~ 1	$\ll 1$	~ 1 or $\ll 1$	$\ll 1$
$\tan\beta$	< 3.5	< 6	> 8	$\in [2, 20]$	> 8
$\lvert\cos\theta_A\rvert$	$\in [0.005, 0.02]$	$\in [0.003, 0.02]$	~ 0	$\in [0.002, 0.017]$	~ 0
m_χ	$\in [80, 200]$	$\in [70, 300]$	< 15	$\in [113, 400]$	$\in [91, 110]$
$\log[\Omega h^2]$	$\in [-0.65, 0.4]$	$\in [-1.9, 1.8]$	$\in [6.3, 7.3]$	~ -1	~ -1
$\log[\sigma_p^{SI}(\text{ pb})]$	$\in [-8.7, -8.2]$	$\in [-10, -7]$	$\in [-14.5, -9.8]$	$\in [-10, -7]$	< -12
χ^2	$\in [26, 70]$	> 10	> 10	$\in [2.7, 26]$	$\in [1.9, 6.0]$

four tau mode, with a third being very close to consistency. However, we have shown that by changing A_κ by a very small amount compared to the nominal value found in the scan (which did not use the ALEPH limit on the four tau final state as an input to the chi-squared employed) will allow consistency with the ALEPH limit without altering any other phenomenology.

As regards the relic density, the Ωh^2 values of the Type I points were not within the two sigma range of the observations, but four out of the five were within a factor of 2 or 3 of $\Omega h^2 \sim 0.1$. Perhaps not too much should be read into this as the relative scarcity of these points in our relaxed-CNMSSM scan could mean our understanding of these parameter points is incomplete. Correct Ωh^2 can be achieved for the Type I points by varying the most relevant gaugino mass parameter (M_2) slightly. However, we found that for M_2 such that the relic density was correct one or more of the LEP Higgs limits was not satisfied.

There was a another very interesting class of points, denoted Type III, that appeared in our relaxed-CNMSSM scan. Type III points are, first of all, characterized by $BR(h_1 \to b\bar{b}) > 0.5$ (*i.e.* the normal SM decay is dominant) and by $m_{a_1} > 2m_B$ (*i.e.* $a_1 \to b\bar{b}$ is dominant). Points satisfying this criterion are, as one might expect, very numerous. Further, we found that it was very easy to find points satisfying the above criteria that gave Ωh^2 values in close agreement ($\pm 2\sigma$) with the observed value (something that we included in our final definition of Type III points, along with the requirement that they obey the ALEPH limits on $h_1 \to a_1 a_1 \to 4\tau$ decays and the BaBar limits on $\Upsilon(3S) \to \gamma a_1$ decays). Within the Type III class, as finally defined, the very best predictions for Ωh^2 were obtained for cases in which the lightest Higgs is very singlet-like with $85 < m_{h_1} < 110$ GeV and the lightest neutralino is very singlino-like with $91 < m_\chi < 110$ GeV. Such scenarios are dubbed SS scenarios. For all such SS scenarios, sufficiently small Ωh^2 in agreement with experiment is achieved via $\chi - \widetilde{\tau}_1$ coannihilation. We believe that one should take these SS scenarios seriously. It will then be the second lightest Higgs boson (predicted to have mass m_{h_2} close to 114 GeV) that has SM-like couplings to WW,ZZ and its decays will also be SM-like. Unfortunately, in such scenarios the spin-independent cross section for direct dark matter detection is predicted to be very small, $\sigma_p^{SI} < 10^{-12}$ pb. Rates for collider production of the singlet-like h_1 will be very low. The χ will appear in chain decays at the LHC and its roughly 100 GeV mass should be measurable with reasonable accuracy. However, to determine how singlet it is would require observation of a displaced vertex. Unfortunately, the predicted non-singlet content of the χ for the SS scenarios is of order $1 - N_s^2 \sim few \times 10^{-6} - 10^{-4}$, sufficient

to make the decays to the χ prompt.

Overall, it is clear that even a slight extension of the strongly constrained CNMSSM to allow non-universality for the Higgs soft-masses-squared and for A_κ opens up the phenomenological possibilities very considerably. One finds fairly good ideal-Higgs-like scenarios. In addition, the very intriguing singlet-scenarios that are consistent with all experimental constraints and give excellent Ωh^2 become quite prominent.

VI. ACKNOWLEDGEMENTS

JFG is supported by US DOE grant DE-FG03-91ER40674. JFG acknowledges support by the Aspen Center for Physics during a portion of this project. The work of R. RdA has been supported in part by MEC (Spain) under grant FPA2007-60323, by Generalitat Valenciana under grant PROMETEO/2008/069 and by the Spanish Consolider Ingenio-2010 program PAU (CSD2007-00060). R. RdA would like to thank the support of the Spanish MICINN's Consolider-Ingenio 2010 Programme under the grant MULTIDARK CSD2209-00064. DEL-F is supported by the French ANR TAPDMS ANR-09-JCJC-0146 and would like to thank the Science Technology and Facilities Council for its support at the beginning of this collaboration. LR is supported by the EC 6th Framework Proramme MRTN-CT-2006-035505 and by the Foundation for Polish Science. TV would like to thank the Science Technology and Facilities Council. The use of the Iceberg cluster is gratefully acknowledged.

[1] R. Dermisek and J. F. Gunion, *The NMSSM Solution to the Fine-Tuning Problem, Precision Electroweak Constraints and the Largest LEP Higgs Event Excess*, Phys. Rev., D76 (2007), p. 095006, [hep-ph/0705.4387].

[2] R. Dermisek and J. F. Gunion, *Consistency of LEP event excesses with an $h \to aa$ decay scenario and low-fine-tuning NMSSM models*, Phys. Rev., D73 (2006), p. 111701, [hep-ph/0510322].

[3] S. Chang, R. Dermisek, J. F. Gunion, and N. Weiner, *Nonstandard Higgs Boson Decays*, Ann. Rev. Nucl. Part. Sci., 58 (2008), pp. 75–98, [hep-ph/0801.4554].

[4] R. Barate et al., *Search for the standard model Higgs boson at LEP*, Phys. Lett., B565 (2003), pp. 61–75, [hep-ex/0306033].

[5] B. A. Dobrescu, K. T. Matchev, JHEP **0009**, 031 (2000). [hep-ph/0008192].

[6] D. E. Lopez-Fogliani, L. Roszkowski, R. R. de Austri, and T. A. Varley, *A Bayesian Analysis of the Constrained NMSSM*, Phys.Rev., D80 (2009), p. 095013, [hep-ph/0906.4911].

[7] C. Balazs, D. Carter, Phys. Rev. **D78**, 055001 (2008). [arXiv:0808.0770 [hep-ph]].

[8] *SuperBayeS*. `http://www.superbayes.org/`.

[9] L. Roszkowski, R. Ruiz de Austri, R. Trotta, Y.-L. S. Tsai, and T. A. Varley, *Some novel features of the Non-Universal Higgs Model*, (2009), [hep-ph/0903.1279].

[10] D. G. Cerdeno, C. Hugonie, D. E. Lopez-Fogliani, C. Munoz, and A. M. Teixeira, *Theoretical predictions for the direct detection of neutralino dark matter in the NMSSM*, JHEP, 12 (2004), p. 048, [hep-ph/0408102].

[11] J. Skilling, *Nested sampling*, AIP Conference Proceedings, 735 (2004), pp. 395–405.

[12] F. Feroz and M. P. Hobson, *Multimodal nested sampling: an efficient and robust alternative to MCMC methods for astronomical data analysis*, (2007), [astro-ph/0704.3704].

[13] R. Trotta, F. Feroz, M. P. Hobson, L. Roszkowski, and R. Ruiz de Austri, *The Impact of priors and observables on parameter inferences in the Constrained MSSM*, JHEP, 12 (2008), p. 024 [hep-ph/0809.3792].

[14] R. R. de Austri, R. Trotta, and L. Roszkowski, *A Markov chain Monte Carlo analysis of the CMSSM*, JHEP, 05 (2006), p. 002, [hep-ph/060202].

[15] L. Roszkowski, R. R. de Austri, and R. Trotta, *On the detectability of the CMSSM light Higgs boson at the Tevatron*, JHEP, 04 (2007), p. 084, [hep-ph/0611173].

[16] L. Roszkowski, R. Ruiz de Austri, and R. Trotta, *Implications for the Constrained MSSM from a new prediction for $b \to s\gamma$*, JHEP, 07 (2007), p. 075, [hep-ph/0705.2012].

[17] G. Belanger, F. Boudjema, A. Pukhov, and A. Semenov, *micrOMEGAs: A program for calculating the relic density in the MSSM*, Comput. Phys. Commun., 149 (2002), pp. 103–120, [hep-ph/0112278].

[18] U. Ellwanger and C. Hugonie, *NMSPEC: A Fortran code for the sparticle and Higgs masses in the NMSSM with GUT scale boundary conditions*, Comput. Phys. Commun., 177 (2007), pp. 399–407, [hep-ph/0612134].

[19] S. Schael et al., *Search for neutral Higgs bosons decaying into four taus at LEP2*, JHEP, 05 (2010), p. 049 [hep-ex/1003.0705].
[20] B. Aubert et al., *Search for a low-mass Higgs boson in $Y(3S) \to \gamma A^0, A^0 \to \tau^+\tau^-$ at BABAR*, Phys. Rev. Lett., 103 (2009), p. 181801 [hep-ex/0906.2219].
[21] , *A Combination of CDF and D0 results on the mass of the top quark*, (2007), [hep-ex/0703034].
[22] W. M. Yao et al., *Review of particle physics*, J. Phys., G33 (2006), pp. 1–1232.
[23] J. P. Miller, E. de Rafael, and B. L. Roberts, *Muon g-2: Review of Theory and Experiment*, Rept. Prog. Phys., 70 (2007), p. 795, [hep-ph/0703049].
[24] A. Abulencia et al., *Measurement of the $B_s^0 - \bar{B}_s^0$ Oscillation Frequency*, Phys. Rev. Lett., 97 (2006), p. 062003, [hep-ex/0606027].
[25] J. Dunkley et al., *Five-Year Wilkinson Microwave Anisotropy Probe (WMAP) Observations: Likelihoods and Parameters from the WMAP data*, Astrophys. J. Suppl., 180 (2009), pp. 306–329, [astro-ph/0803.0586].
[26] T. Aaltonen et al., *Search for $B_s^0 \to \mu^+\mu^-$ and $B_d^0 \to \mu^+\mu^-$ decays with $2fb^{-1}$ of $p\bar{p}$ collisions*, Phys. Rev. Lett., 100 (2008), p. 101802 [hep-ex/0712.1708].
[27] R. Dermisek and J. F. Gunion, *New constraints on a light CP-odd Higgs boson and related NMSSM Ideal Higgs Scenarios*, Phys. Rev., D81 (2010), p. 075003, [hep-ph/1002.1971].
[28] R. Dermisek and J. F. Gunion, *Direct production of a light CP-odd Higgs boson at the Tevatron and LHC*, Phys. Rev., D81 (2010), p. 055001, [hep-ph/0911.2460].
[29] E. Aprile et al., *First Dark Matter Results from the XENON100 Experiment*, Phys. Rev. Lett., 105 (2010), p. 131302, [astro-ph.CO/1005.0380].
[30] C. E. Aalseth et al., *Results from a Search for Light-Mass Dark Matter with a P- type Point Contact Germanium Detector*, (2010), [astro-ph.CO/1002.4703].
[31] R. Bernabei et al., *New results from DAMA/LIBRA*, Eur. Phys. J., C67 (2010), pp. 39–49, [astro-ph.GA/1002.1028].
[32] D. Hooper, J. I. Collar, J. Hall, and D. McKinsey, *A Consistent Dark Matter Interpretation For CoGeNT and DAMA/LIBRA*, (2010), [hep-ph/1007.1005].
[33] J. F. Gunion, A. V. Belikov, and D. Hooper, *CoGeNT, DAMA, and Neutralino Dark Matter in the Next-To-Minimal Supersymmetric Standard Model*, (2010), [hep-ph/1009.2555].